ABSTRACT

SCHALLER, CHRISTOPHER R. A Model for Propeller Induced Neutral Point Shifts on a Small Electric UAS. (Under the direction of Dr. Charles Hall.)

Since unmanned aerial systems (UAS) have grown in popularity both in civil and military applications, there is a need to fill the gaps in knowledge of design of these system and the development of tools to aid in that design. Since the scale of UAS is generally smaller than that of other light aircraft the effects of different aspects of aircraft design on the stability characteristics of the UAS become more significant. One such area exists in the effects of power on the neutral point of the aircraft. The neutral point of the aircraft must be determined analytically during design in order to control the stability characteristics of the UAS. Estimates for the shift due to power were outlined by Perkins and Hage in their classic text on stability and control of aircraft. This estimate was correlated using WWII Fighters and nothing on the scale of UAS being developed today. Earlier work at North Carolina State University with the Optikos and Phoenix UAS designed and developed by students determined the power-off and power-on neutral points for their aircraft. Their power-off neutral points were within a percent of the mean aerodynamic chord predicted by CMARC analysis. The power-on neutral point was shifted between 2.5 and 3 times the amount predicted by Perkins and Hage. These vehicles were tested with only one propeller. Another small electric powered UAS has been developed, the Astraeus UAS, which has separate wing configurations for high speed and low speed flight, each with differing area, span, and mean aerodynamic chord. Flight testing with both configurations of Astraeus and the previously developed Optikos UAS was conducted with a variety of propellers to determine the effect of the propeller normal force on the location of the neutral point. The effects of varying both the disk diameter and the pitch of the propeller were examined. Neutral point shift results were compared to Perkins and Hage predictions to determine if a change to their model will produce more accurate results. Through more generalized equations developed by Etkin and Reid, neutral point shift results were used to determine the coefficient of the propeller normal force based on the varying propeller geometry. During the course of flight testing with Astraeus, a close coupling effect between the propeller and elevator arose which affected the perceived static margin of the aircraft. This effect was previously assumed to be negligible. The Optikos UAS does not experience this close coupling effect. Shift results from this aircraft indicate that the efficiency of the propulsion system may have a more significant effect on the propeller normal force than simply varying the geometry of the propeller.

A Model for Propeller Induced Neutral Point Shifts on a Small Electric UAS

by
Christopher R. Schaller

A thesis submitted to the Graduate Faculty of
North Carolina State University
in partial fulfillment of the
requirements for the Degree of
Master of Science

Aerospace Engineering

Raleigh, North Carolina

2011

APPROVED BY:

Dr. Ashok Gopalarathnam	Dr. Fred DeJarnette

Dr. Charles Hall
Chair of Advisory Committee

DEDICATION

To my Mother who taught me to never give up, to my Father who showed me how to be a man worth respecting, and to all that have knowing or unknowingly supported me throughout the years, whose names are too numerous to list here.

Thank You!

BIOGRAPHY

Christopher Robbins Schaller was born in 1985 to Christopher Leigh and Elizabeth Schaller in Reading, Pennsylvania. Having spent his formative years in New Canaan, Connecticut, he attended Bucknell University where he earned his Bachelor's degree in Mechanical Engineering. After graduation, he went to Havelock, North Carolina where he would work at MCAS Cherry Point on reliability projects for Navy helicopters. At the end of 2009, he was accepted to and began attending North Carolina Sate University, earning his Master's degree in Aerospace Engineering. He joined the University's Flight Research Group at the start of 2011, where he was a teaching and research assistant working with the senior design classes of 2011 and 2012.

ACKNOWLEDGEMENTS

I would like to thank Dr. Hall in particular for saying yes when everybody else was saying no and for his help and support in teaching me about this world that I had essentially no knowledge of. I can easily say that my short time with him and Flight Research was the most formative year of my higher education.

I would also like to thank the Senior Class of 2011 for tolerating me as their TA while they did the hard stuff. The long days, nights and vacation days spent in the lab were made tolerable due to the excellent company. Learning from you all and being able to help where I could is an experience I would never trade.

And finally to my compatriots in Flight research past and present, Lars Soltmann (my excellent test pilot), Trent Young, Robert Armes, Alex Manasa, and Stearns Hienzen for assisting in the research and data gathering, being there to bounce ideas off of, and showing me the ropes of flight research. You all bring some much needed sunshine to that windowless room.

TABLE OF CONTENTS

LIST OF TABLES

LIST OF FIGURES

Chapter 1

Introduction

1.1 Motivation

The popularity of the Unmanned Aerial System (UAS), as both a military and civil platform, has increased significantly in the past decade. In addition to not needing a pilot inside the aircraft, the UAS as a platform boasts enhanced endurance and ceiling characteristics as compared to manned vehicles of the same size. Because of these benefits, non standard designs and experimental features are often explored on an unmanned aircraft, similar to the testing of small scale models in a wind tunnel before producing a full scale vehicle. These differences in both mission and design imply a need to examine both design methodology and analysis tools for aircraft on this scale. In the case of wing and control surface sizing, the methods used to design larger aircraft may simply be scaled to fit the UAS. Beyond this however, conventional methods for manned aircraft can be modified to improve handling and performance characteristics. Take for example the static margin of the aircraft which determines control powers and many handling qualities. The static margin is defined as the distance between the center of gravity (CG) and the neutral point (NP) located as a percentage of the mean aerodynamic chord of the wing. The neutral point in this context is the aerodynamic center of the aircraft, or more technically the point about which all longitudinal moments about the CG, from lifting surfaces and other sources, no longer change with angle of attack. Modern commercial jets are designed to have static margins above 25%. The margin is large to allow for shifts in the CG due to fuel use and passenger movement. In these jets a shift of 5% in either direction will not impact the pilot's ability to control the aircraft in any significant way. If these jets were designed with a tighter range on static margin, say 10%, a 5% shift in either direction would have a significant effect on both the control powers of the aircraft and the handling qualities. In a commercial application the benefit to the large static margin, in addition to the ability to move the CG around, is increased stability in all flight modes. There are, however, benefits to smaller static margins for different applications. In general the smaller static margin improves several performance aspects of aircraft by reducing the

downforce on the tail. This reduces the amount of lift that the main wing (in a conventional aircraft) would need to produce to keep itself aloft which in turn reduces the amount of drag being generated, improving fuel economy. In the small electric UAS, the static margin determines the CG range for stability and control. Reducing the design static margin reduces these required CG limits. For these vehicles this can result in less required space in the fuselage, reducing material needed and reducing the weight of the aircraft. The lower static margin means more control power is available to the pilot, resulting in more agile aircraft.

The neutral point is determined analytically during the design of the aircraft using the following equation[1, p. 32].

$$h_n = h_{n_{wb}} - \frac{a_t}{a}\overline{V}_H\left(1 - \frac{\partial \epsilon}{\partial \alpha}\right) - \frac{1}{a}\frac{\partial C_{m_p}}{\partial \alpha} \tag{1.1}$$

This equation includes contributions from the wing-body, the horizontal stabilizing surfaces, the downwash effect from the wing to the tail, and the effect of the propulsive unit. Panel code analysis tools such as CMARC can give reasonable estimations of the power off neutral point including the the effect of downwash ($\frac{\partial \epsilon}{\partial \alpha}$). In the equation above, $\partial C_{M_p}/\partial \alpha$ represents the effect of the propulsion system on the neutral point. For the small electric UAS, there are two primary propulsive effects to consider. The moment generated by a difference in the thrust line of the propulsion system and the vertical location of the CG is well known as it is an easily measurable force and moment arm. The second effect is unique to propeller driven aircraft and is the normal force generated by a spinning propeller. This force is non-inertial and perpendicular to the axis of rotation of the propeller. If the propeller's axis of rotation is in-line with the x axis of the aircraft, the normal force will point in the negative z direction relative to the aircraft's orientation. In Phillips' *Mechanics of Flight* the coefficient of the normal force is defined as being dependent on the propeller blade geometry, the number of blades, and the advance ratio of the propeller in flight[2, p. 184-190]. Analysis of this force via wind tunnel testing is very difficult due to the sensitive force measuring equipment required to decouple the measurement of the normal force from thrust line effects, the torque of the motor, and any other asymmetric forces such as the p-factor. It is due to these factors there is very little data available on the normal force generated by the propeller and as a result no reliable estimation for its effect on the neutral point. If a reliable estimation of the effect of the propeller on the NP were available, more accurate information regarding the static margin of the completed aircraft will help determine control powers and handling effects well before the aircraft is ever flown. With this information in hand, the safety of first flight is greatly improved.

1.2 Research Overview

The Flight Research Group at North Carolina State University uses UAV's as platforms for research into stability and controls, aerodynamic forces in flight, propeller design, lifting surface design, and alternative configuration development. For this project, two aircraft generated from NCSU's aerospace senior design program were used. The senior design program is a pair of courses taking place over a student's final academic year in which small groups of students design, build, and test a UAS to a specific set of customer requirements. These aircraft are electrically powered and are designed to use folding propellers. Through flight testing of these aircraft it is possible to apply methodology developed for full size manned aircraft for the determination of the neutral point. Flight data was collected for the design configurations of both aircraft in both powered and unpowered flight so as to determine the power off and power on neutral point. The difference between these two neutral points is a direct measurement of the effect of the normal force since these aircraft were designed with no thrust line effects. As it is expected that the magnitude of the normal force will change with propeller geometry, flight testing will be conducted using propellers varying pitch and diameter independently from the design configuration. By comparing the neutral point shift due to a change in propeller geometry (either constant diameter while varying pitch or constant pitch while varying diameter) a model for the effect of the normal force based on geometry can be developed.

There are several benefits to using the small electric UAS as a platform for this research. The weight of the aircraft will not change in flight due to fuel burn; the weight of the battery remains constant while discharging. Additionally, the location of the CG will remain constant as long as internal components are secured against movement due to flight maneuvers. Due to the nature of the electric motor as compared to a gasoline engine, the propeller is trivial to restart after powering off the aircraft in flight, this fact allows us to easily determine the power off neutral point through flight testing.

1.3 Previous Work

Previous work on the propeller's effect on the neutral point is fairly sparse. It is referenced in several texts on stability and control of aircraft but often just referred to and never explored. In their seminal text on stability and control Perkins and Hage refer to the effects of the propeller as "...(only possible) to account for only parts of these effects analytically with any degree of accuracy, so that complete analysis of the power or propeller effects is done more or less qualitatively at the present time (1949)"[3, p. 232-235]. The text goes on to give a qualitatively derived relation for the effect of the propeller's normal force based on data collected from World War II era fighter aircraft.

$$\left(\frac{dC_m}{dC_l}\right)_{N_p} = .02\frac{l_p}{c} \tag{1.2}$$

Where l_p is the distance from the CG to the propeller disk and c represents the length of the mean aerodynamic chord of the wing. Since none of the data used for the development of this model is available, several assumptions can be made about the source aircraft. A majority of World War II fighter aircraft from the late 1940's were tractor configuration, gasoline powered, and employed the use of constant speed propellers. Vehicles on the scale of the small electric UAS are far too small to be equipped with constant speed propeller systems which are often complex and extremely heavy compared to the rest of the aircraft. It is not surprising, therefore, to learn that this estimation of the neutral point shift due to the propeller is not generally applicable.

More modern texts on longitudinal stability such as that by Etkin and Reid generalize the change in pitching moment due to the propeller's normal force as follows[1, p. 69].

$$\frac{\partial C_{m_p}}{\partial \alpha} = \frac{S_p}{S} \frac{x_p}{\bar{c}} \frac{\partial C_{N_p}}{\partial \alpha_p} \frac{\partial \alpha_p}{\partial \alpha} \tag{1.3}$$

In this equation, $\frac{x_p}{\bar{c}}$ is the same as Perkins and Hage's $\frac{l_p}{c}$ and $\frac{\partial \alpha_p}{\partial \alpha}$ represents the downwash like effect experienced by the propeller's change in angle of attack with respect to the change in angle of attack of the aircraft. The coefficient of the propeller normal force must in this case be determined through experimentation in the wind tunnel to determine the magnitude of the force for a given velocity and angle of attack. Comparing this to Perkins and Hage, the World War II fighter given as example would have a value of .02 for $\frac{S_p}{S} \frac{\partial C_{N_p}}{\partial \alpha_p} \frac{\partial \alpha_p}{\partial \alpha}$.

Previous work with NCSU senior design aircraft Optikos and Phoenix (2009) determined the power on and power off neutral point of both aircraft. The power off neutral point locations calculated from flight testing were within 3% of the estimated value from CMARC analysis[4, 5]. This provided the primary motivation for this research.

The goal of this research is threefold. Firstly, to examine the propeller induced shift on the neutral point for any trends based on changing the propeller geometry. Secondly, the shift data will be used to determine if a Perkins and Hage style model for the neutral point shift could be developed. Thirdly, through the generalized equation developed by Etkin and Reid to determine $\frac{\partial C_{N_p}}{\partial \alpha_p} \frac{\partial \alpha_p}{\partial \alpha}$ based on the power shift results and develop a model for this coefficient.

Chapter 2

Methodology

2.1 Theory

Generally, both manned and unmanned aircraft are designed to posses static stability. This means that when disturbed from a stable condition such as constant speed at a constant altitude the aircraft will tend to return to that condition. Longitudinal static stability is determined entirely by the relationship between the center of gravity and the aerodynamic neutral point. If the neutral point is located aft of the center of gravity, the resulting pitching moment from disturbing the aircraft from a stable condition will be negative, indicating a return to the stable condition. If the neutral point were to be located at the center of gravity, the aircraft would be considered neutrally stable and any disturbance from the stable angle of attack will not result in any pitching moment on the aircraft. Finally, if the neutral point were to be located forward of the center of gravity, the aircraft is considered unstable and the resulting pitching moment from a disturbance would cause the aircraft to move farther away from the stable condition. Analytical determination of the neutral point accounting for propulsive effects is typically not done due to the lack of a cohesive model for the effect of the normal force. As a result, determination of the true neutral point is typically done during the course of flight testing for new aircraft. This is accomplished through practical application of longitudinal stability theory to data collected in flight.

According to theory, pitch stability (dC_m/dC_L) can be related to elevator angle deflection (δ_e) by the following relation[6, p. 224].

$$\frac{d\delta_e}{dC_L} = \frac{(dC_m/dC_L)}{C_{m_{\delta_e}}} \tag{2.1}$$

From this equation, the neutral point is defined as the CG location that will set $d\delta_e/dC_L$ equal to zero. When the CG is at this location the aircraft is considered neutrally stable and the control powers for the aircraft become infinite. As this makes the aircraft unsafe, a different method for determining the neutral point is often employed. In trim level flight, the elevator deflection is given by the following

equation.

$$\delta_{e_{trim}} = -\frac{C_{m_0} C_{L_{\delta_e}} + C_{m_\alpha} C_{L_{trim}}}{C_{L_\alpha} C_{m_{\delta_e}} - C_{L_{\delta_e}} C_{m_\alpha}} \tag{2.2}$$

In horizontal flight δ_e becomes a unique function of $C_{L_{trim}}$ (and thus aircraft speed) for a particular CG location. Differentiating with respect to $C_{L_{trim}}$ results in the following equation.

$$\frac{d\delta_{e_{trim}}}{dC_{L_{trim}}} = -\frac{C_{L_\alpha}}{C_{L_\alpha} C_{m_{\delta_e}} - C_{L_{\delta_e}} C_{m_\alpha}} (h - h_n) \tag{2.3}$$

During trim and level flight of the aircraft, airspeeds and elevator deflections of the aircraft are collected. Knowing the local weather conditions and altitude at which data was collected, the airspeed is then converted to a $C_{L_{trim}}$. Data collection is repeated for at least three CG locations allowing for the plotting of $\delta_{e_{trim}}$ vs $C_{L_{trim}}$, more commonly referred to as the trim curves of the aircraft. A common intercept for the trim curves is then determined representing the constants in Equation 2.3. The slopes of these lines are then be plotted vs CG location, resulting in a plot of $d\delta_{e_{trim}}/dC_{L_{trim}}$. Extrapolating via linear regression will allow the x-intercept of the resulting line to be determined. From stability theory this point is the neutral point of the aircraft.

2.2 Aircraft Overview

For this research, two aerial vehicle platforms developed by in North Carolina State University's capstone senior design course were used for data collection, the Optikos UAS and Astraeus UAS. Both are small electrically powered pusher configuration vehicles whose CG location can be varied by shifting of the flight battery and/or the addition or removal of ballast. Each has a pitot-static tube mounted on the aircraft nose far enough away from the fuselage as to minimize body effects on the measurement of static pressure. Each aircraft is designed with the thrust line of the propulsion system passing through the location of the CG. This ensures that the propeller normal force is the only propulsive contribution to C_{m_α}.

Optikos is a flying wing developed by seniors in the class of 2009. Their specific design challenge was that both the aircraft and a bungee launching system that could be broken down and transported in a defined volume case. Optikos' design configuration features an 11x8 folding propeller. The power off neutral point location was initially determined by CMARC analysis as 18.07%$m.a.c$ and through flight testing was determined to be 15.6%$m.a.c$[4].

The Astraeus UAS is a standard (forward wing and aft tail) configuration aircraft developed by seniors of the class of 2011. The design challenge for this year was to design the aircraft with two separate wing configurations, a high speed wing for greater speed and maneuverability, and a low speed wing for enhanced endurance. Each wing is attached to a common fuselage and since the

Figure 2.1: Optikos UAS

neutral point is determined mostly by lifting surfaces, each configuration can be studied separately for the purpose of this research. Both Astraeus configurations employ a 14x9.5 folding propeller. There is no available CMARC analysis of the power off neutral point for Astraeus, however AVL analysis was conducted to determine the static margin for the design configuration and two additional CG locations [7]. Details on each aircraft's design are contained in the appendix.

Flight testing was conducted with both aircraft using their design propeller configurations to determine both the power on and power off neutral point. For the purpose of this research additional testing was conducted using propellers of varying disk area and pitch angle to determine each parameter's effect on the neutral point shift. Testing for Optikos employed the use of the following propeller geometries: 12x8, 10x8, 11x7, and 11x9. Both Astraeus configurations were flown with the following additional propellers: 14x10, 14x8.5, 15x10, and 13x10. As the power off neutral point is not affected by the propulsion system in flight, only the power on neutral point was determined for the non-design propellers.

(a): High Speed Configuration

(b): Low Speed Configuration

Figure 2.2: Astraeus UAS

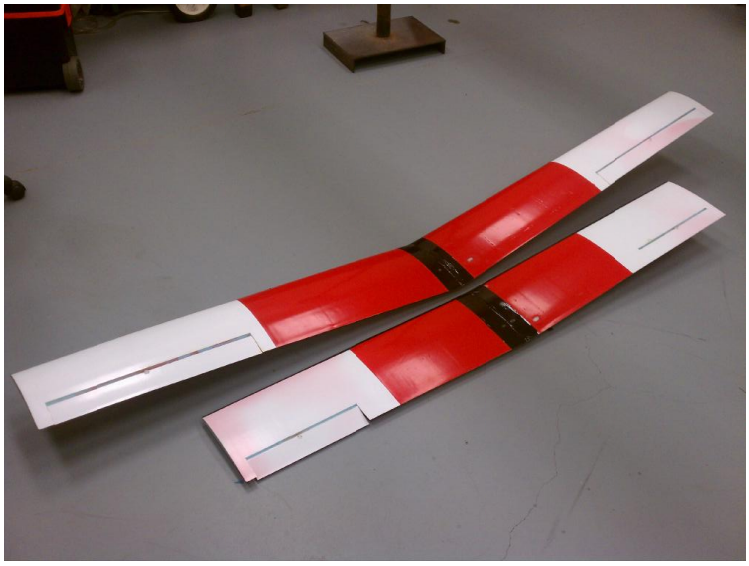

Figure 2.3: Astraeus UAS Wing Comparison

2.3 Data Collection

Flight test data for both aircraft was collected using the Eagle Tree Flight Data recorder which collects data at a rate of 10 samples a second.

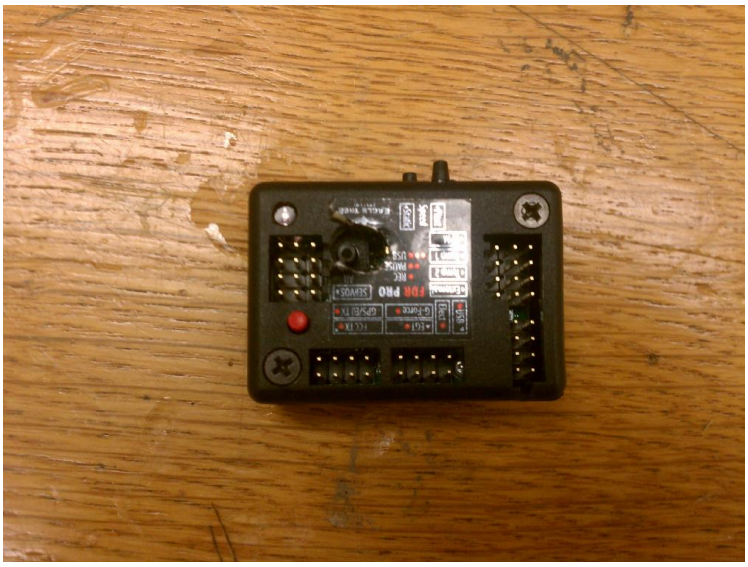

Figure 2.4: Eagle Tree Flight Data recorder

This data recorder is a powered in flight by the battery via the aircraft's RC receiver. It contains two transducers for measuring the altitude and indicated airspeed of the aircraft via the pitot-static tube. The transducers can be damaged by pressures of roughly one inch of Mercury of either positive or negative pressure and this range is not exceeded by the flight profile of these aircraft. Of relevance to this research, when connected to the aircraft's RC receiver it can measure the pulse width modulation (PWM) signal being sent from the RC controller to the servomotors that displace the control surfaces. Servomotor position cannot itself be recorded, so instead the recorder collects the the input signal from the RC transmitter which is commanded by the pilot. The actual data recorded by the unit is a scaled value based on the bit length available to the on-board software and thus must be calibrated to convert the signal being recorded to the actual deflection seen by the control surface. This is accomplished by recording the signal collected by the recorder for known deflections as determined by shining a laser on a mirror attached to the control surface and measuring its displacement on a wall a known distance away. This method is represented graphically in Figure 2.5. As the PWM signal length for deflection is not a perfectly linear relation in the relevant range Gaussian interpolation was used to generate calibration equations. Since trim for these aircraft occurs at small angles of attack, only the relevant range of elevator deflections is considered. Calibration curves for both aircraft are presented in Figure 2.6 using the convention of down elevator (moving the control stick forward)

being a positive deflection. The calibration curves represent the true deflection of the elevators and are not shifted for any trim condition.

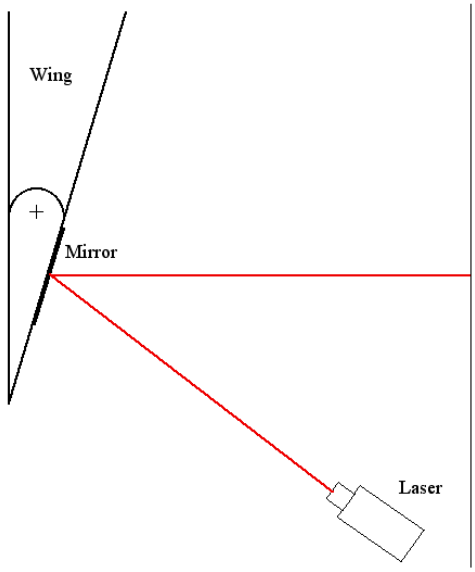

Figure 2.5: Graphical Depiction of Control Surface Calibration Setup

The recorder is also able to collect thermocouple data, RPM data, g-force data, GPS position, current drawn by the motor, and remaining voltage on the flight battery. Via a 900 MHz transmitter, airspeed, altitude, and other data can be sent to the ground station via the Seagull telemetry system, also by Eagle Tree Systems [8]. The Seagull telemetry unit is used at the ground station to assist the pilot in setting the trim condition of the aircraft. After each flight, data is downloaded from the recorder at the ground station using Eagle Tree proprietary software which saves the data as a text file. All data collected while the aircraft is in the trim condition is considered steady state.

2.4 Flight Test

Relevant data recorded in flight for this research is done in trimmed level flight at varying speeds and thus varying elevator deflection angles [6, p. 230]. The trim condition is set by the pilot for a given speed. For this research, flights were conducted with the aircraft flown via digital proportional radio control from the ground station. The requirements for data collection are trimmed level flight at a constant speed wherein the trim condition is set by the external pilot. A real time data display tied into the flight recorder is used to assist in the determination of speed and altitude for data flights.

Of what is recorded by the Eagle Tree unit during flight, the following are the relevant data needed for neutral point determination.

1. Indicated Airspeed

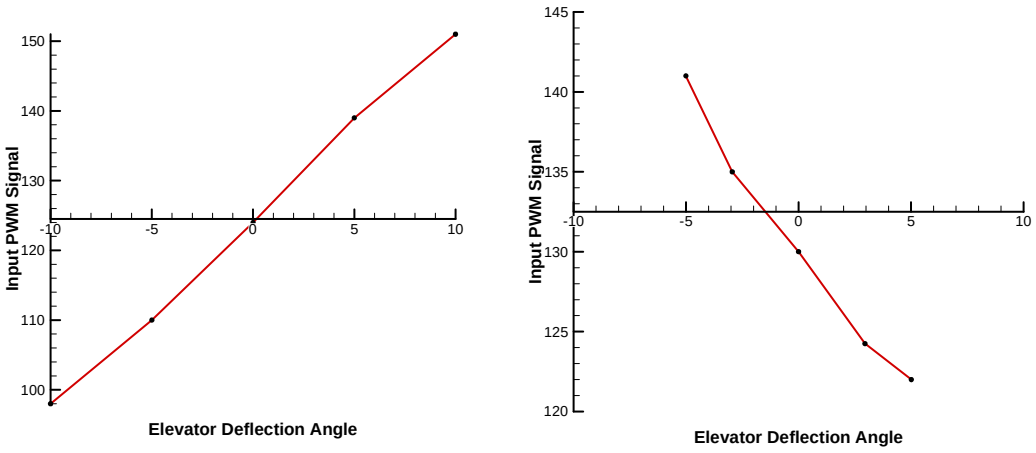

(a): Astraeus Calibration Curve

(b): Optikos Calibration Curve

Figure 2.6: Calibrated Elevator Deflections for Astraeus and Optikos (Relevant Range)

2. Altitude

3. Elevator Deflection

Weather data such as local barometric pressure, weather station altitude, ambient air temperature, and dew point temperature are also required for data analysis but since flights are conducted at low altitudes above ground level (AGL) temperature remains constant throughout the flight envelope. Local barometric pressure does vary with altitude; however, the change in local air density is negligible within the flight envelope of the aircraft being used (see Section 2.4.1 for detailed analysis). Since the data is time stamped, variations in temperatures and barometric pressures during the course of the flight testing day can be accounted for via online almanacs for the reference weather stations.

To ensure the safety of the ground crew and any spectators a list of standard procedures was adhered to during flight testing. These procedures outline steps to be taken from arrival on site to initial launch as well as steps for collection of data and inspection procedures after landing. Before leaving for a flight, the aircraft were balanced to ensure that the longitudinal locations of the CG are known and to set the desired static margins. The aircraft were also re-balanced to incorporate any changes incurred due to necessary repairs or changes to the propeller being used as prescribed by the flight test being conducted. Weights for the aircraft at each CG location are also collected to be used in the data reduction. One of the beneficial aspects of the electric UAS is that since there is no consumption of fuel, the aircraft weight and CG location remain constant during flight.

Flights were conducted over a large field free from obstructions to ensure enough time for the pilot to set the trim condition before needing to maneuver the aircraft. After either hand launch or bungee assisted launch the external pilot would do a few circuits and adjust the settings on the RC

transmitter as necessary to aid in flight. At the ground station an assistant (the flight test engineer or FTE) would constantly call out airspeeds as indicated by the real time recorder display. Data collection start and end points were set by the pilot and marked in the raw data via a switch on the RC controller. This switch sends a constant signal to the receiver on board the aircraft which is collected by the data recorder. A second FTE would be manually recording flight times and average speeds over the course of a data run to determine the next data point to be collected. Data is collected for eight to ten speeds at trim condition. After the data is collected the pilot safely lands the aircraft where the data is downloaded at the ground station and the CG location can be changed (often by relocating the aircraft battery) prior to the next flight. This data is collected for three known CG locations within the CG limits of the aircraft.

In order to determine power off neutral point, data collection was repeated with the pilot setting the trim condition after throttling back to zero. In these small electric UAS, the motor electromagnetically brakes the drive shaft, preventing the propeller from windmilling. To eliminate the drag from the stationary propeller a folding propeller must be employed. When not spinning, the propeller blades fold, in the case of Astraeus and Optikos, completely in line with the fuselage or tail boom and out of the flow. When the propeller blades are folded back they do affect the longitudinal location of the CG but this delta can be neglected as it is very small due to the low weight of the propeller blades. Since the motor is off during data collection, there is no additional thrust available to keep the aircraft at a constant altitude so power off data is collected during a much shorter window as compared to the power on regime.

Flight test cards used for this research are attached in the appendix. These cards outline procedures for the preparation and execution of flight testing as well as physical data collection areas for the ground station crew.

2.4.1 Sources of Error

The Eagle Tree Flight Recorder is not a perfect system. It is designed to be a low cost alternative to laboratory quality data collection systems. Altitudes measured by the Eagle Tree unit used on Astraeus were often unreliable. The first few flights would record acceptable altitude readings, but as time progressed, the recorded data was invalid, usually recording a static value for altitude of zero or a negative number. Testing with the aircraft revealed that the static port and line work correctly, and that the static pressure accurately feeds into the determination of airspeed, but due to either software or hardware error/malfunction, altitude data was not available for analysis. As a result of this a standard local density was used based on a 200 feet AGL flight envelope which is the ceiling beyond which the aircraft becomes too small to accurately control. Data was analyzed assuming that the local density at altitude was the same as the ground station, which was determined by local weather conditions and base altitude. Error analysis for a single data point is presented in Table 2.1 for this

assumption. The baseline conditions used are a barometric pressure of 29.92 $inHg$, air temperature of 68°F, a base altitude (altitude of weather station) of 488 ft, and a dew point temperature of 62°F. Since data is collected in level flight at a low altitude and compressibility effects are neglected, the indicated airspeed is not affected by this error.

Table 2.1: Altitude Error Analysis

Condition	Density (lb/ft^3)	δ_e (deg)	Equivalent Airspeed (ft/s)	$C_{L_{trim}}$
0 ft AGL	0.0733	4.875	45.92	0.4763
200 ft AGL	0.0728	4.875	45.92	0.4796
Difference=.69%				

Since the flight recorder does not directly measure the position of the servomotor but rather the pilot's input, it is sensitive to the pilot's movements. This sensitivity is seen in the data as a variance in the measured signal length even when the control surface is held at a constant deflection. To counteract this, an average over the range where the altitude and speed for the data set are constant was taken for determining the surface deflection. Communication between the ground station and the pilot regarding the aircraft's speed and altitude allows the external pilot to more accurately set the trim condition and ensure good data points. Wind and other weather effects can disrupt the aircraft's trim condition and level flight regime, though any wind strong enough to affect the aircraft's speed and heading is easily recognizable by the external pilot and these data runs can be excluded from analysis.

Chapter 3

Results

3.1 Flight Testing

A total of 46 flights were conducted with Optikos and both Astraeus configurations including repeat data flights as needed. The course of flight testing included three flights per propeller used, one for each designed CG location. For Astraeus, flight testing included the design 14x9.5 propeller in both configurations as there was no previous data available. Power on and power off neutral point data for Optikos was determined by the senior class of 2009 and is used in the data analysis presented in this research in an effort to reduce the number of flights required. As these aircraft were designed with folding propellers, there were a few issues that arose when they were flown with fixed propellers. Primary among these issues was in landing, there was a chance that the motor would brake in a position where the tip of the propeller would strike the ground before any landing skid on the fuselage. On Astraeus this would often result in the pitot tube being buried in the ground or simply torn off the aircraft. Additionally, the long tail boom configuration could create a very large moment arm capable of shearing the motor mount from its attachment to the aircraft. To reduce the chance of damage to the aircraft, in the course of flight testing the motor mount was strengthened and the pitot tube relocated. Figure 3.1 shows the change made to the pitot tube for Astraeus. It was assumed that since it is a thin object that does not extend vertically far from the fuselage profile that the additional drag generated would be negligible. After these changes were made and after any repairs, the aircraft was balanced to ensure that the CG locations remained consistent throughout testing and new weights were collected to be used in the data reduction. The vertical location of the CG was shifted by a marginal amount and the resulting thrust line effects were assumed to be negligible. Through the course of testing, the lifting surfaces and fuselage, major contributors the location of the neutral point, suffered no ill effects.

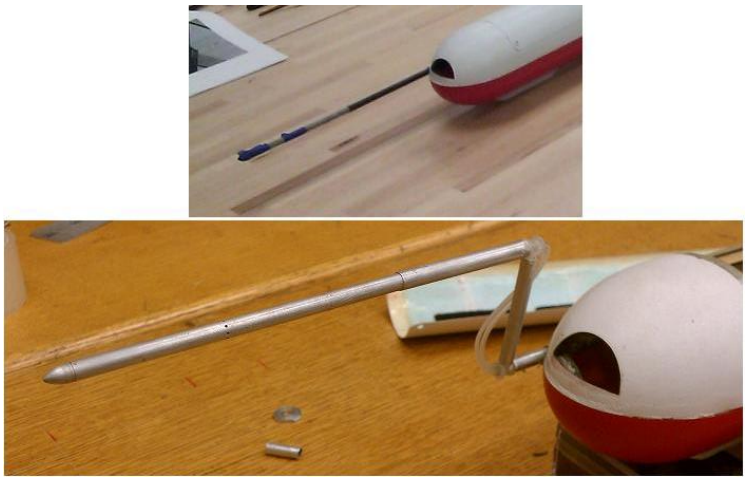

Figure 3.1: Original and Relocated Astraeus Pitot Tube

3.2 Data Reduction

Flight recorder data from each flight was downloaded and labeled after landing to reduce the chance of lost data. There was only one incidence of data lost to user error, unfortunately there was not time available to repeat this data flight. The raw data files are space delimited and the relevant data channels from the recorder were extracted for reduction. This data is then reduced to generate a plot of $d\delta_e/dC_L$ vs. CG location for the aircraft in terms of percentage of the mean aerodynamic chord ($\%m.a.c$) which will give us the location of the neutral point as the x intercept of the linear regression equation prescribed by the three data points.

The indicated airspeed (IAS) of the aircraft is first converted from miles per hour (mph) into feet per second and then into equivalent airspeed (V_e) by the following equation

$$V_e = IAS(\rho/\rho_0)^{(1/2)} \tag{3.1}$$

Where ρ is the local density as determined by local barometer, base altitude, air temperature, and altitude of the aircraft, and ρ_0 is the standard seal level density. Since flights were done at low altitudes and low Mach numbers, compressibility effects can be neglected and the equivalent airspeed can be regarded as the true airspeed of the aircraft. The trim lift coefficient ($C_{L_{trim}}$) is then determined by the following equation.

$$C_{L_{trim}} = \frac{W}{\frac{1}{2}\rho_0 V_e^2 S} \tag{3.2}$$

Where W is the gross weight of the aircraft and S is the area of the wing planform. Using the calibration curves for the aircrafts elevator (or in the case of Optikos, elevons), the PWM signal of

the elevator channel is converted into a true deflection. Within the data run indicated by the marker channel, average deflection angles and $C_{L_{trim}}$ values are extracted and stored in a separate data file. As a rule only data runs where there are many data points at a constant speed and altitude are used in the analysis. Microsoft Excel was used in the data reduction, converting elevator input signals into deflections according to the calibration curves and using weather data, altitude (if available) and speed to determine $C_{L_{trim}}$. Within the marked sections of data the trim condition was identified as a constant speed over several seconds coupled with a marginal (less than 10ft) delta in altitude if altitude information was available. To ensure that good data points were being used, the trim data was plotted before linear regression to see if there was a positive linear trend at each CG location.

The δ_e vs. $C_{L_{trim}}$ data must be plotted forcing a common intercept for all three CG locations. This common intercept is given below, which represents the constant terms in Equation 2.2.

$$\frac{-C_{L_\alpha} C_{m_0}}{C_{L_\alpha} C_{m_{\delta_e}} - C_{L_{\delta_e}} C_{m_\alpha}} \tag{3.3}$$

Since it is assumed that this common intercept is a constant value for each CG location, it may be determined via a linear least squares regression of the trim data collected from flight testing. Mathematically we can convert Equation 2.2 into the following form.

$$\delta_{e_{i,j}} = a + b_i C_{L_{trim_{i,j}}} \tag{3.4}$$

In Equation 3.4, a is the common intercept, and b the slope of the $d\delta_e/dC_{L_{trim}}$ curve. The index i represents the CG location, and j the index of the data collected for that CG location. Equation 3.4 now represents a linear system of equations for the trim condition of the aircraft at three CG locations, represented by the matrix equation below.

$$\begin{Bmatrix} \delta_{e_{1,j}} \\ \delta_{e_{2,j}} \\ \delta_{e_{3,j}} \end{Bmatrix} = \begin{bmatrix} 1 & C_{L_{trim_{1,j}}} & 0 & 0 \\ 1 & 0 & C_{L_{trim_{2,j}}} & 0 \\ 1 & 0 & 0 & C_{L_{trim_{3,j}}} \end{bmatrix} \begin{Bmatrix} a \\ b_1 \\ b_2 \\ b_3 \end{Bmatrix}$$

By performing the pseudo-inverse of the $C_{L_{trim}}$ matrix and post multiplying it by the δ_e vector the values for a and b_i are determined. The elevator trim curves for the three CG locations are now plotted and the slopes of those curves are plotted vs. the corresponding CG location. A simple linear regression of the $\partial\delta_{e_{trim}}/\partial C_{L_{trim}}$ points results in an equation whose x-intercept is the location of the neutral point for that data set. A MATLAB program was written which performs this linear least squares regression on the trim data for the aircraft. The program outputs plots of the three trim curves for the aircraft as well as a plot of the $\partial\delta_e/\partial C_{L_{trim}}$ versus h or CG location in terms of $\%m.a.c$. Figure 3.2 contains sample trim curves and neutral point locater plot generated by the regression code. The

MATLAB code used to produce these curves is contained in the appendix.

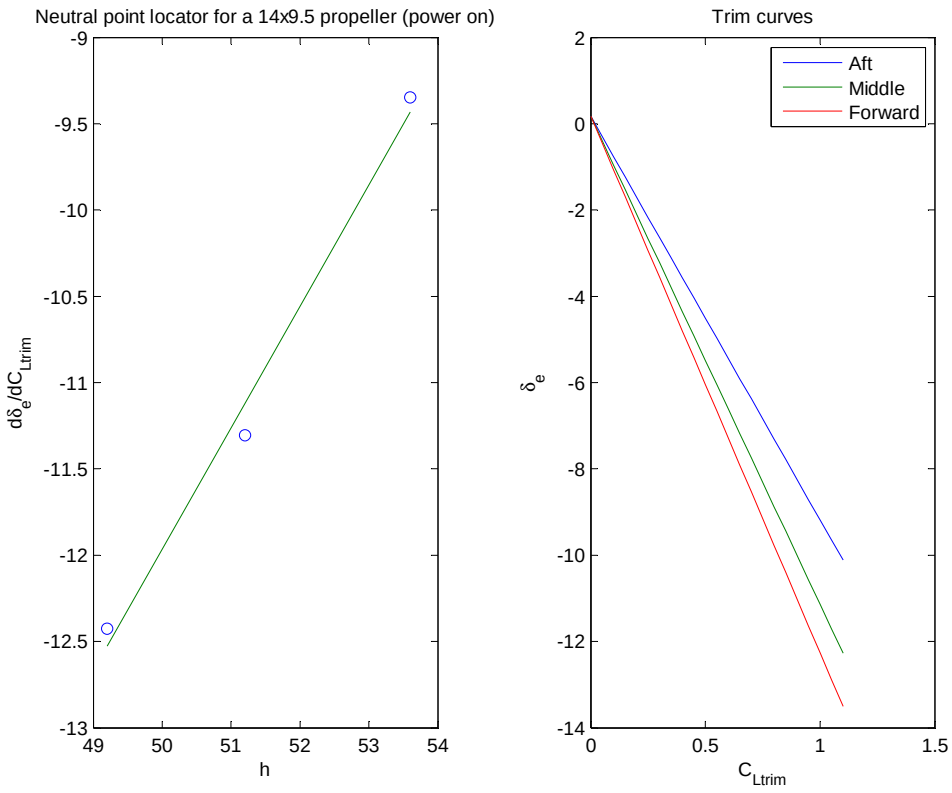

Figure 3.2: Sample Results from Linear Regression of Data

Sign conventions used in the data reduction indicate that the expected trend is a negative slope for $d\delta_{e_{trim}}/dC_{L_{trim}}$ which increases in magnitude as the static margin is increased. Bad data points would show themselves as being far outside the trend, or a trend that indicated a negative static margin (positive slope).

The numerical results were stored in a spreadsheet file for analysis, the output figures saved for inclusion in this document (see Appendix C). For each, if a repeat reduction produced a new result, this result would replace the previous.

The figures and numerical results were examined prior to analysis to determine the fidelity of the data reduction. The expectation from the linear regression was increasingly negative slopes of the trim curves as the static margin is increased. Since the CG locations for both Astraeus and Opitkos are evenly spaced, the delta for slopes of the trim curves should be reasonably consistent. A poor result would show itself as either exceptionally wide or narrow spacing between the trim curves, or poor curve fitting on the neutral point locater. In these cases, the data reduction was re-examined and then reanalyzed. In the case of repeatedly poor results, the MATLAB code can be adapted to perform

the linear regression with only two sets of data points, excluding the CG location data that was far from the mean. This does reduce the confidence in the results where this two point analysis has been performed, however these results are more believable. In this research when a result was obtained using two point analysis instead of three, special note is made in the presentation and both the two point and three point result is included in Appendix C.

3.3 Results

Tables 3.1, 3.2, and 3.3 present both power on and power off locations of the neutral point for all three aircraft as well as the resulting delta, with a positive value indicating an aft-ward shift. All values are given in $\%m.a.c$ of the aircraft. MATLAB output figures for each propeller are attached in Appendix C.

Table 3.1: Neutral Point Shift Results of the Low Speed Astraeus UAS

Diameter	Pitch	Power On	Power Off	Shift	Notes
13	10	56.12	55.76	.36	
14	8.5	60.01	55.76	4.25	2 Point Analysis
14	9.5	64.19	55.76	8.43	Design Propeller
14	10	66.51	55.76	10.75	2 Point Analysis
15	10	70.39	55.76	14.63	2 Point Analysis

Table 3.2: Neutral Point Shift Results of the High Speed Astraeus UAS

Diameter	Pitch	Power On	Power Off	Shift	Notes
13	10	61.80	65.36	-3.56	2 Point Analysis
14	8.5	58.31	65.36	-7.05	
14	9.5	67.01	65.36	1.65	Design Propeller
14	10	60.82	65.36	-4.54	
15	10	63.70	65.36	-1.66	2 Point Analysis

Table 3.3: Neutral Point Shift Results of Optikos UAS

Diameter	Pitch	Power On	Power Off	Shift	Notes
10	8	12.60	15.6	-3.45	2 Point Analysis
11	7	19.16	15.6	3.56	
11	8	25.68	15.6	10.08	Design Propeller
11	9	19.34	15.6	3.74	
13	8	7.61	15.6	-7.98	Pusher Style Prop

Chapter 4

Analysis

4.1 Trends in Neutral Point Shifts

To determine if any trends arose in in the neutral point shifts determined through flight testing, the values of the shifts were plotted on the basis of constant disk diameter (Figure 4.1) and constant pitch (Figure 4.2).

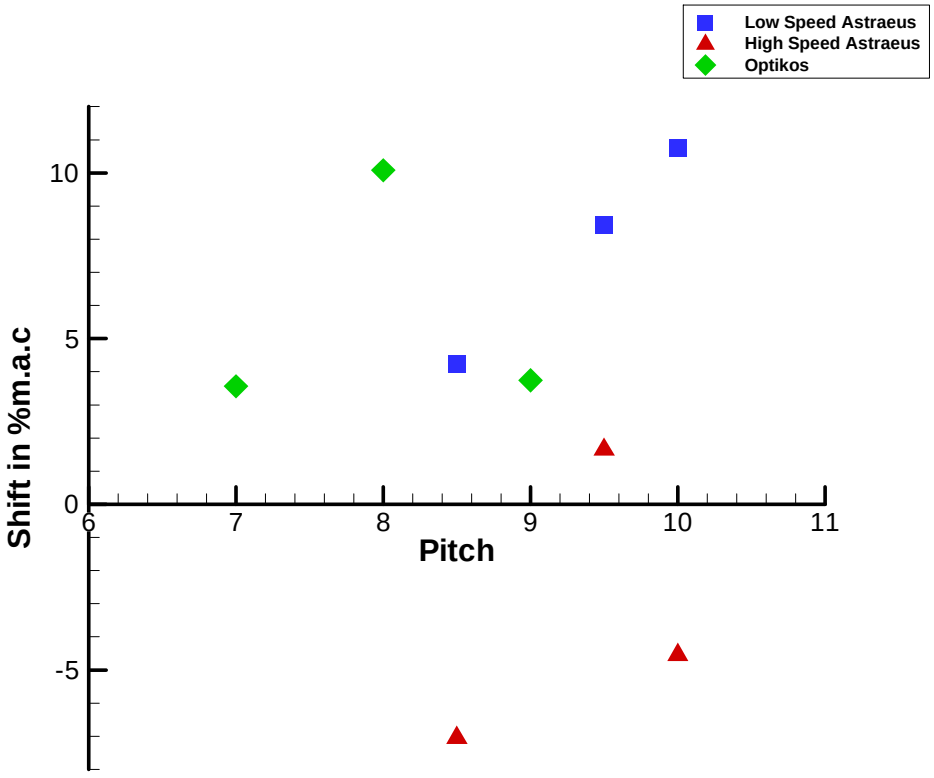

Figure 4.1: Neutral Point Shift Results for Constant Disk Diameter

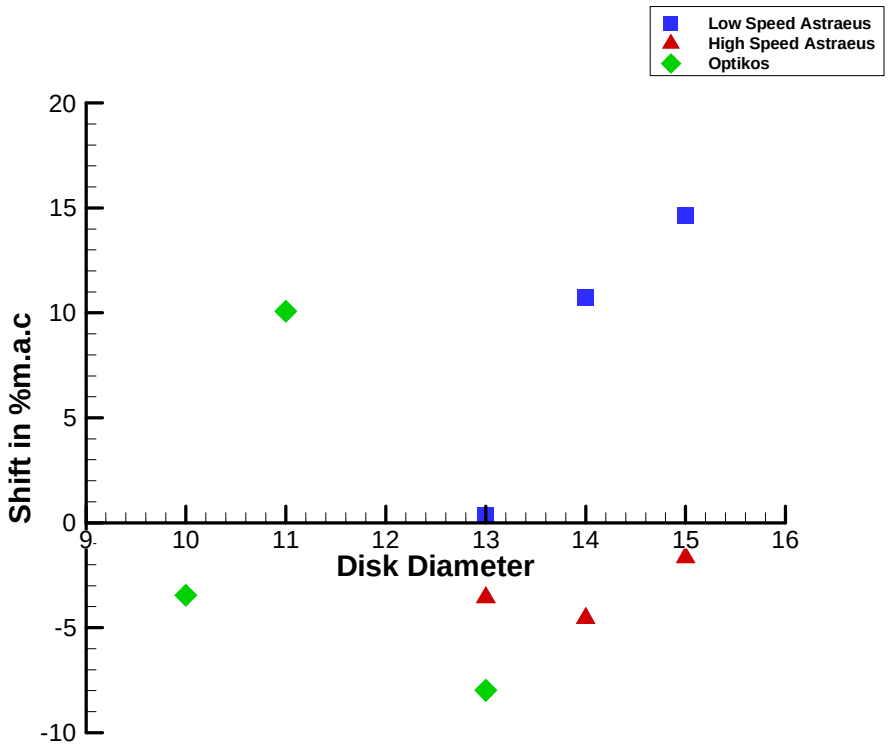

Figure 4.2: Neutral Point Shift Results for Constant Pitch

The results for the High Speed Astraeus and Optikos indicate that the shift in the neutral point peaks for the design propeller. As Astraeus uses 10 inches as the constant pitch versus the design of 9.5 inches, this result is unconfirmed on a constant pitch basis. Unlike the other two, the low speed Astraeus indicates a linearly increasing trend in both constant disk diameter and constant pitch. One might expect this this result due to the fact that as the pitch or diameter is increased from a base value, more thrust is being generated at a constant RPM. Since propeller blade theory links the normal force to the thrust of the propulsion system, it is not unreasonable to expect this linear relation. However, as this result is not repeated in either the high speed configuration or in Optikos, that conclusion is suspect. The propellers for the design configuration of each aircraft were chosen to be the most efficient across all flight regimes. These results therefore indicate a stronger relationship to the efficiency of the propulsion system rather than the geometry of the specific propeller. This agrees with theory and analysis presented by Phillips in his discussion of propeller dynamics[2, p. 184-190].

4.2 General Analysis

It is well established in longitudinal stability theory that in a pusher configuration the propeller normal force will be a stabilizing effect and a destabilizing effect for a tractor configuration. This means that for the three aircraft used in this research, it is expected that all the shifts in the neutral point will be aft-ward (positive by convention). The results of this research indicate that this is not consistently the case. However, rather than discount decades of proven research it is more likely that there is an aspect of the aircraft used that has been unaccounted for. The motor on the Astraeus UAS is very close to the horizontal tail, which relative to the size of the wing is very small. This close coupling of the motor and tail generates a previously neglected effect on the longitudinal stability characteristics of the aircraft. The spinning propeller induces an increased dynamic pressure on the tail. This additional dynamic pressure increases the forces and moments generated by the elevator deflection, giving more control authority than if the motor was off. Mathematically the additional induced dynamic pressure is represented by an unknown variable, $\Delta\eta$. The result of this increased dynamic pressure on the elevator is a perceived reduction in the static margin of the aircraft. The static margin is not expected to change as a result of the increased dynamic pressure, the aircraft merely sees more control authority in the elevator. This additional control authority will effect the results of flight testing by moving the power on neutral point much farther forward than expected. Mathematically, the effect of the induced dynamic pressure is seen in the equations for trim (reference Equations 2.2 and 2.3).

$$\frac{d\delta_{e_{trim}}}{dC_{L_{trim}}} = -\frac{C_{m_\alpha}}{C_{L_\alpha}C_{m_{\delta_e}} - C_{L_{\delta_e}}C_{m_\alpha}} = -\frac{C_{L_\alpha}(h-h_n)}{C_{L_\alpha}C_{m_{\delta_e}} - C_{L_{\delta_e}}C_{m_\alpha}} \tag{4.1}$$

$$\frac{-C_{m_\alpha}}{(1+\Delta\eta)[C_{L_\alpha}C_{m_{\delta_e}} - C_{L_{\delta_e}}C_{m_\alpha}]} = \left(\frac{h-h_n}{1+\Delta\eta}\right)\frac{-C_{L_\alpha}}{C_{L_\alpha}[C_{m_{\delta_e}} - C_{L_{\delta_e}}(h-h_n)]} \tag{4.2}$$

In the right side of Equation 4.2 the C_{L_α} terms will cancel out and since $[C_{L_\alpha}C_{m_{\delta_e}} - C_{L_{\delta_e}}C_{m_\alpha}]$ and $[C_{m_{\delta_e}} - C_{L_{\delta_e}}(h-h_n)]$ are constants for the aircraft, as the pitch stiffness is decreased by a factor of $1/(1+\Delta\eta)$ so is the static margin by the same factor. Reducing the static margin means that the power on neutral point is perceived as being much closer to the CG. This effect is present most significantly in the results for the high speed Astraeus. The results from the low speed Astraeus are affected by this close coupling, however the fact that neutral point shifts determined through flight testing were aft-ward indicates that the coupling effects are dependent on the speed of the aircraft.

Since the pilot is now controlling an aircraft with a perceived static margin different than the physical static margin the flight test methodology for determining the neutral point for aircraft with this close coupling is essentially invalid. The perceived increased control powers means that the pilot needs to input less elevator deflection for trim at a given speed and since the effect is not linearly dependent on speed, the magnitude of the increase in control powers will vary across all flight regimes.

This close coupling is present in Astraeus whenever the motor is spinning. It is expected, therefore, that the power off neutral points determined through flight testing are reasonable values. Optikos does not experience this close coupling as its motor is farther from the lifting surface (which is itself larger in comparison to the Astraeus tail), and the elevator deflection does not affect the flow path into the prop.

4.3 Comparison With Perkins and Hage

When comparing to the prediction from Perkins and Hage the design location for the CG is used to determine l_p/c. This dependence on only the aircraft geometry indicates that the geometry of the propeller should have no influence on the location of the neutral point. Tables 4.1,4.2, and 4.3 show the predicted values from the Perkins and Hage equation in comparison with the flight tested value and the difference between the two. All data apart from the propeller geometry is $\%m.a.c$. These results show that there is indeed a dependence on the propeller geometry, in fact there were only three instances where the Perkins and Hage prediction was within 2% of the $\%m.a.c$ of the value determined from flight testing. There is no apparent trend that would indicate a coefficient modification to the Perkins and Hage prediction would make it more accurate.

Table 4.1: Low Speed Astraeus Perkins and Hage Comparison

Low Speed Astraeus				
Diameter	Pitch	Shift	P&H Prediction	Difference
13	10	.36	7.23	6.87
14	8.5	4.25	7.23	2.98
14	9.5	8.43	7.23	-1.20
14	10	10.75	7.23	-3.52
15	10	14.63	7.23	-7.40

Table 4.2: High Speed Astraeus Perkins and Hage Comparison

High Speed Astraeus				
Diameter	Pitch	Shift	P&H Prediction	Difference
13	10	-3.56	6.78	10.34
14	8.5	-7.05	6.78	13.83
14	9.5	1.65	6.78	5.13
14	10	-4.54	6.78	11.32
15	10	-1.66	6.78	8.44

Table 4.3: Optikos Perkins and Hage Comparison

Optikos				
Diameter	Pitch	Shift	P&H Prediction	Difference
10	8	-3.45	2.71	6.16
11	7	3.56	2.71	-0.85
11	8	10.08	2.71	-7.37
11	9	3.74	2.71	-1.03
13	8	-7.12	2.71	9.83

4.4 Determination of $C_{N_{p\alpha}} \frac{\partial \alpha_p}{\partial \alpha}$

Knowing the value of S_p/S from the geometry of each aircraft we can determine the unknown factors in the relation developed by Etkin and Reid (Equation 1.3). As the form of this equation is linear, the results are scaled values of those presented in section 4.1 and are plotted for constant disk diameter and constant pitch diameter in Figures 4.3a and 4.3b.

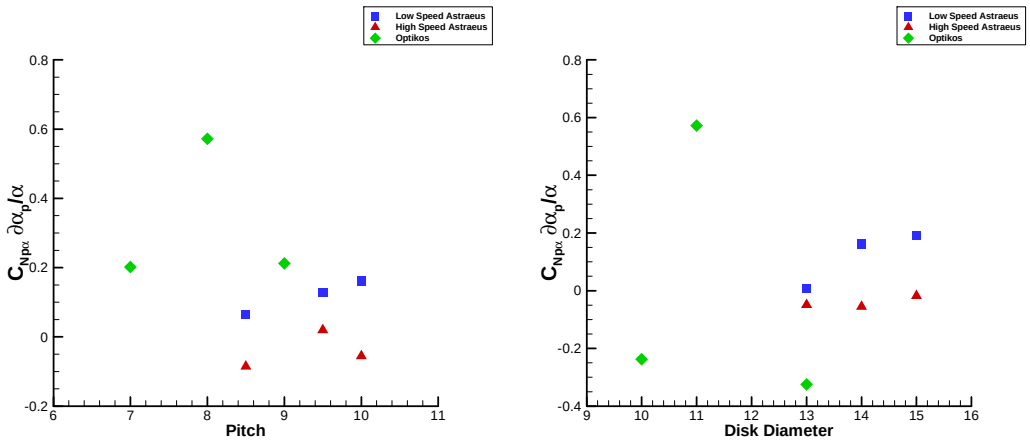

(a): Constant Disk Diameter

(b): Constant Pitch

Figure 4.3: Plots of $C_{N_{p\alpha}} \frac{\partial \alpha_p}{\partial \alpha}$

Chapter 5

Conclusions

5.1 Concluding Remarks

The goal of this research was to determine if a better model for the effect of the propeller normal force on the location of the neutral point for a small electric UAS could be found. Unfortunately due to aspects of the test aircraft's geometry previously assumed to be negligible, confidence in the results presented in is low. The analytical difficulties created by the close coupling of Astraeus prevent further flight testing from being effective for this research. Further flight testing with Optikos or similar aircraft without the close coupling effects may reveal more of the nature of the propeller normal force. The results from this research, however, indicate that the design propellers for small electric UAS are chosen for a reason; their high efficiency resulting in a more significant effect on the location of the neutral point. This agrees with theory presented by Phillips and others regarding propeller dynamics.

5.2 Future Work

With a larger sample size of propellers it would be possible to develop a more definitive model of $C_{N_{p_\alpha}}$ for a particular aircraft. Ensuring that the close coupling of the horizontal tail and motor that Astraeus experienced was not present in future aircraft will increase the confidence in any results obtained through further flight testing. Additionally, this research was conducted using only pusher configuration aircraft. The equations governing the propulsive effects on the neutral point assume that as long as the motor is the same distance from the CG, the only difference between a pusher and tractor configuration is a change of sign. Previous work in NCSU senior design did develop aircraft that could switch propulsion configuration within a given period of time. Unfortunately neutral point data for these aircraft is not available for analysis. Furthermore, the result from Perkins and Hage was obtained using "typical WWII era fighter planes" which, for the most part, were powered by constant speed propellers. The propellers used for this research were fixed pitch as constant speed systems

are too large for the scale of the small UAS. Since constant speed propellers can vary their pitch to improve the efficiency of propulsion in a given flight regime, it stands to reason that values for $C_{N_{p_\alpha}}$ and certainly $\partial \alpha_p / \partial \alpha$ would change for the same aircraft by fixing the pitch. Similarly, a propeller that is free to pitch at speed would develop a different coefficient of the normal force in different flight regimes. Unfortunately due to the complexity and difficulty of implementing a constant speed or free to pitch propeller system on a small electric UAS, other methods will need to be employed to explore these avenues of neutral point research.

Based on the results of this research, in further work on a model for $C_{N_{p_\alpha}}$ it may be beneficial to examine the propeller normal force separate from the aircraft. Extensive wind tunnel testing across a large range of propeller geometries and manufacturers may generate a better model. By ensuring that measurements are taken when the propeller is operating at high efficiency, the most significant effects of the propeller normal force can be explored. Aircraft flight testing coupled with CMARC analysis can then be conducted to support those results via neutral point shifts. Experimental determination of the propeller normal force, however, comes with its own slew of difficulties the most prominent of which being decoupling the measurement of the normal force from measurement of thrust line effects in the wind tunnel.

Further experimentation with Astraeus may reveal more about the close coupling effects, such as the determination of $\Delta\eta$. From discussions with those who have piloted Astraeus and examination of the trim data at various speeds, the close coupling likely has a non-linear relation with the speed of the aircraft. The elevator's effect on $\partial \alpha_p / \partial \alpha$ could also be explored as the control surface runs the width of even the largest propeller used in this research.

REFERENCES

[1] B. Etkin and L. D. Reid, *Dynamics of Flight Stability and Control*. John Wiley and Sons, Inc., 1996.

[2] W. F. Phillips, *Mechanics of Flight*. John Wiley and Sons, Inc., 2004.

[3] C. D. Perkins and R. E. Hage, *Airplane Performance Stability and Control*. John Wiley and Sons, Inc., 1950.

[4] A. Stewart, J. Brown, W. Diehl, A. Doutov, M. Hastings, K. Kennedy, L. Soltmann, and T. Young, "Optikos: Final Report." 2009.

[5] T. Brucki, D. Dudley, B. Hiteshew, J. McGowan, A. Parker, J. Rodio, and J. Scoggins, "Phoenix: Final Report." 2009.

[6] R. D. Kimberlin, *Flight Testing of Fixed-Wing Aircraft*. American Institute of Aeronautics and Astronautics, Inc., 2003.

[7] R. Armes, J. Baysden, S. Carter, C. Gibson, J. O'neal, L. Pittman, R. Stanford, and W. Sterrett, "Astraeus: Final Report." 2011.

[8] E. T. S. LLC, "Product Manual." `http://eagletreesystems.com`, July 2011.

APPENDICES

Appendix A

Aircraft Geometry

A.1 Optikos UAS

Table A.1: Optikos Surface Geometry

Optikos Aircraft Geometry			
Wing		Winglet	
Airfoil	Eppler 171 Modified	Airfoil	Flat Plate
Span	5.6 ft	Height Above Wing	7.2 in
Area	5.07 ft^2	Height Below Wing	2.4 in
Tip Chord	10.9 in	Area (Total)	167.7 in^2
Root Chord	10.9 in	Sweep	37.5 deg
Aspect Ratio	5.9	Root Chord	11 in
Sweep	25 deg	Upper Tip Chord	5.5 in
		Lower Tip Chord	9.19 in

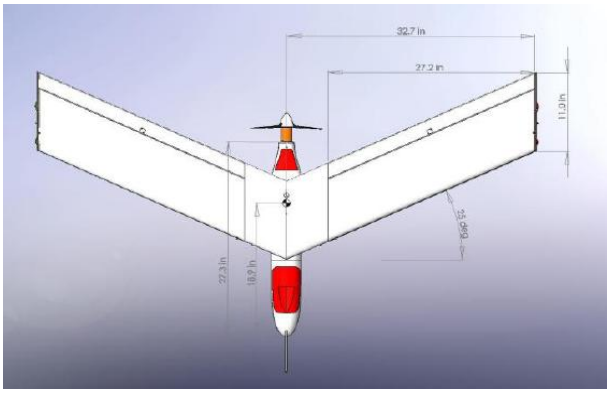

Figure A.1: Optikos: Top View

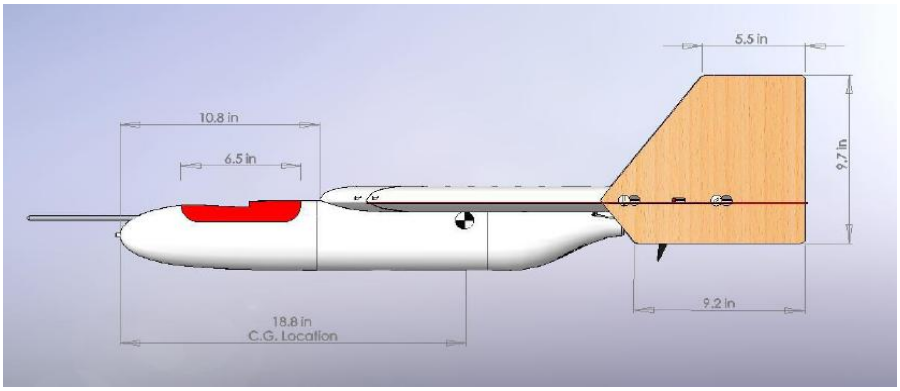

Figure A.2: Optikos: Side View

A.2 Astraeus UAS

Table A.2: Astraeus Geometry

Astraeus Geometry			
Low Speed Wing		High Speed Wing	
Airfoil	MH115	Airfoil	MH30
Root Chord	10 in	Root Chord	10 in
Tip Chord	8 in	Tip Chord	9 in
Span	93 in	Span	66 in
Area	837 in^2	Area	627 in^2
Aspect Ratio	10.3	Aspect Ratio	7
Sweep	-.62 deg	Sweep	-.43 deg
Horizontal Tail		Vertical Tail	
Airfoil	NACA 0012	Airfoil	NACA 0012
Root Chord	7 in	Root Chord	7 in
Tip Chord	4.5 in	Tip Chord	5 in
Span	30 in	Span	9.8 in
Area	173 in^2	Area	72 in^2
Aspect Ratio	5.2	Aspect Ratio	2
Sweep	5.5 deg	Sweep	7.1 deg
L_t	25.5 in	L_v	25.4 in
Winglets			
	Airfoil	NACA 0012	
	Root Chord	4.5 in	
	Tip Chord	3 in	
	Span	6 in	
	Area	45 in^2	
	Aspect Ratio	0.8	

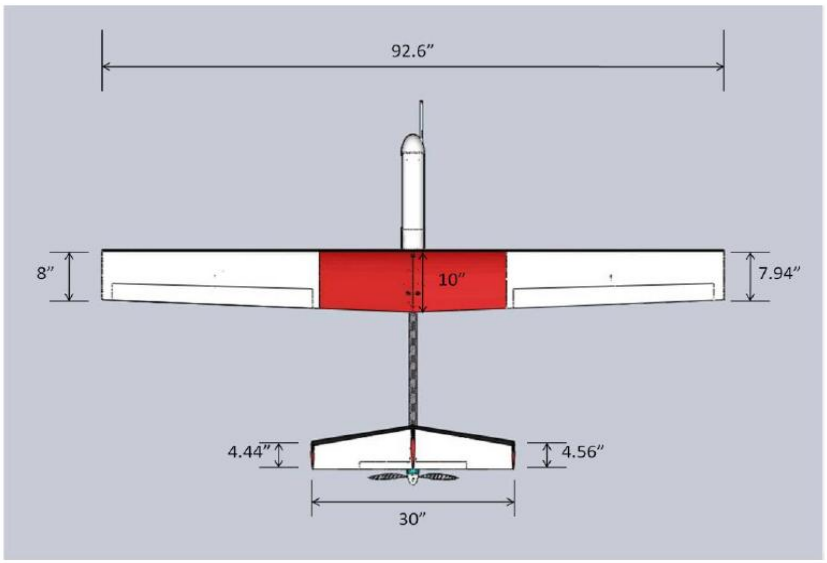

Figure A.3: Astraeus Low Speed: Top View

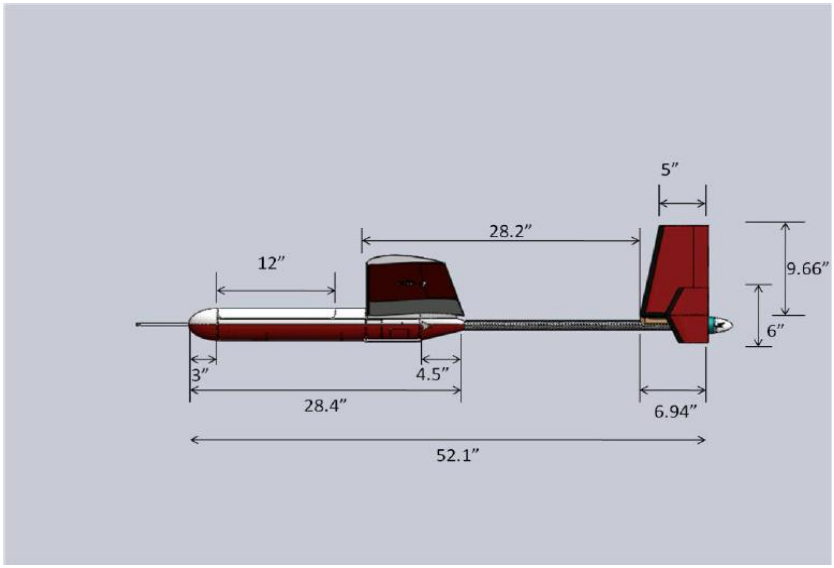

Figure A.4: Astraeus Low Speed: Side View

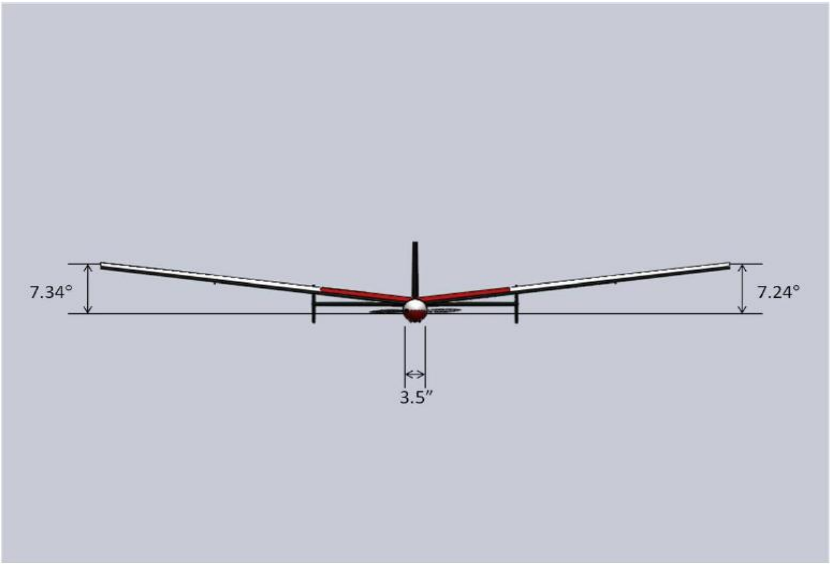

Figure A.5: Astraeus Low Speed: Front View

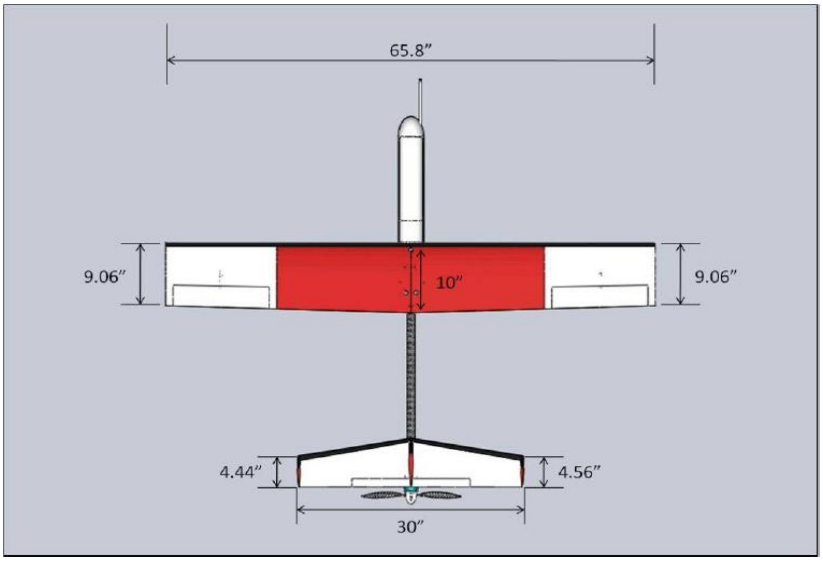

Figure A.6: Astraeus High Speed: Top View

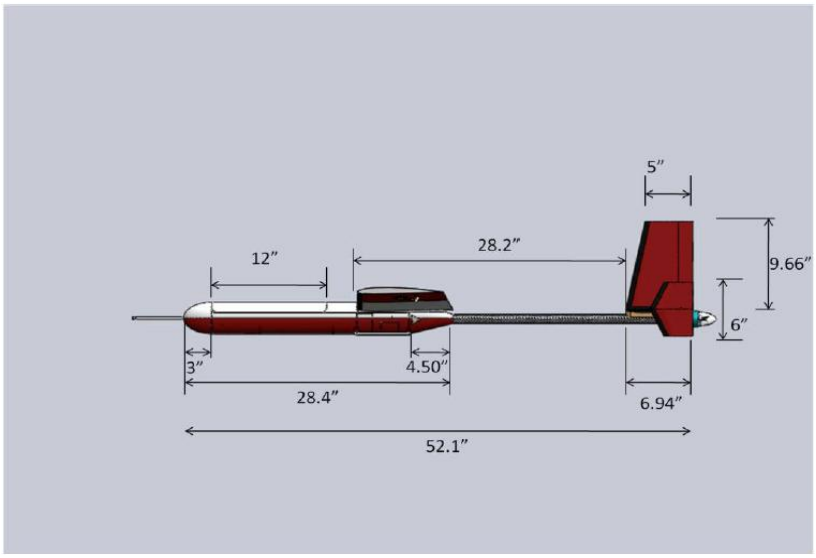

Figure A.7: Astraeus High Speed: Side View

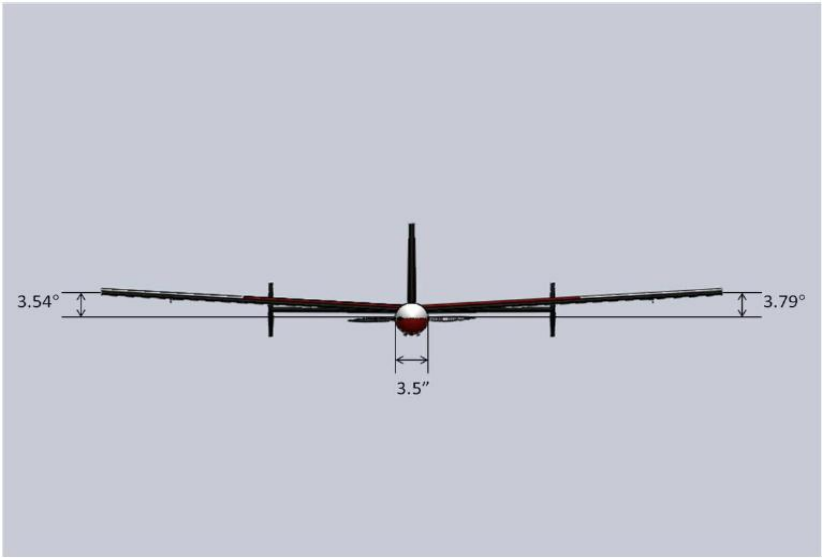

Figure A.8: Astraeus High Speed: Front View

Appendix B

Documentation

B.1 MATLAB Code for Data Analysis

```
%Calculation of regression equation for determining neutral point (power on
%or power off)

q=input('enter 1 for power on, 2 for power off, 3 for debug ');

if q==1
    data_raw_on = xlsread('Name of input data file.xls', 'On');
    i=data_raw_on(1,4);     %number of points at lowest static margin
    j=data_raw_on(1,5);     %number of points at middle static margin
    k=data_raw_on(1,6);     %number of points at highest static margin
    forward=data_raw_on(2,4); %lowest sm cg location
    middle=data_raw_on(2,5); %middle sm cg location
    aft=data_raw_on(2,6); %highest sm cg location
    diameter=data_raw_on(3,4); %prop diameter
    pitch=data_raw_on(3,5); %prop pitch
elseif q==2
    data_raw_off = xlsread('Name of input data file.xls', 'Off');
    i=data_raw_off(1,4);     %number of points at lowest static margin
    j=data_raw_off(1,5);     %number of points at middle static margin
    k=data_raw_off(1,6);     %number of points at highest static margin
    forward=data_raw_off(2,4); %lowest sm cg location
    middle=data_raw_off(2,5); %middle sm cg location
    aft=data_raw_off(2,6); %highest sm cg location
```

```
    diameter=data_raw_off(3,4); %prop diameter
    pitch=data_raw_off(3,5); %prop pitch
end

cg_1=forward;
cg_2=middle;
cg_3=aft;

%array creation

del_e=zeros(i+j+k,1);
trim=zeros(i+j+k,4);
m_array=zeros(4,1);

%fill arrays
if q==1
    for z=1:i+j+k
        del_e(z)=data_raw_on(z,1);
        trim(z,1)=1;
    end
    for x=1:i
        trim(x,2)=data_raw_on(x,2);
    end
    for p=1:j
        trim(p+i,3)=data_raw_on(p+i,2);
    end
    for r=1:k
        trim(r+i+j,4)=data_raw_on(r+i+j,2);
    end
elseif q==2
    for z=1:i+j+k
        del_e(z)=data_raw_off(z,1);
        trim(z,1)=1;
    end
    for x=1:i
        trim(x,2)=data_raw_off(x,2);
    end
```

```
    for p=1:j
        trim(p+i,3)=data_raw_off(p+i,2);
    end
    for r=1:k
        trim(r+i+j,4)=data_raw_off(r+i+j,2);
    end
end


%perform pseudo inverse on trim array
pseudo_trim=pinv(trim);

%fill result array
m_array=pseudo_trim del_e



%plots
xval_cg=[cg_3, cg_2, cg_1];%
for b=1:3
    yval_np(b)=m_array(b+1);
end
linfit=polyfit(xval_cg,yval_np,1);
f=polyval(linfit,xval_cg);
%calculate intercept
neutral_point=-linfit(2)/linfit(1)
subplot(1,2,1)
plot(xval_cg,yval_np,'o',xval_cg,f,'-')
title(['Neutral point locator for a ',...
    num2str(diameter),'x',num2str(pitch),' propeller'])
xlabel('h')
ylabel('d\delta_e/dC_L_t_r_i_m')
axis auto
axis xy
clear n
for n=1:i
    del_e_1(n)=del_e(n);
```

```
    trim_1(n)=trim(n,2);
end
clear n
for n=1:j
    del_e_2(n)=del_e(n+i);
    trim_2(n)=trim(n+i,3);
end
clear n
for n=1:k
    del_e_3(n)=del_e(n+i+j);
    trim_3(n)=trim(n+i+j,4);
end
x=0:.05:1.1;
y_1=m_array(2)*x+m_array(1);
y_2=m_array(3)*x+m_array(1);
y_3=m_array(4)*x+m_array(1);
subplot(1,2,2)
plot(x,y_1,x,y_2,x,y_3)
legend('Aft','Middle','Forward')
title('Trim curves')
xlabel('C_L_t_r_i_m')
ylabel('\delta_e')
axis auto
axis xy
```

B.2 Flight Test Cards

Aircraft Checklist/Mission plan

Date _____

Pilot _____
Additional Personnel

_____

_____

_____

Pre-Flight

1. Visual inspection of aircraft
2. Power/range/surface check
3. Ensure seagull is functional
4. Assemble and inspect launcher if necessary

Flight prep

1. Assemble aircraft with fresh battery
2. Power on transmitter, throttle at mid
3. Connect battery
4. Reset eagle tree
5. Start stopwatch
6. Cycle surfaces (elevator, aileron, rudder, gear)
7. Arm ESC
8. Place aircraft on launcher/prepare for hand launch
9. Countdown
10. Launch

In flight

1. Power up, climb up and away from launch area
2. Establish data circuit course
3. Trim aircraft as needed
4. Perform circuits until pilot is ready for data collection
5. Collect time on stop watch, weather data set is power on or off, and average speed of run
6. Click in gear switch on pilot cue and click out on pilot cue
7. Repeat at various speeds and power settings
    a. 10 data runs per power setting hoping to repeat each average speed

Landing/recovery

1. Disconnect battery
2. Power off transmitter
3. Inspect aircraft for damage
4. Prepare for next flight

Data sheets for flight testing

Weather information

RDU			WRAL		
Barometer	temp	altitude	Barometer	Temp	Altitude

A/C		Flight #		Propeller	
Datapoint	on/off	Speed	Time	CG Location	
1					
2					
3					
4					
5					
6					
7					
8					
9					
10					

A/C		Flight #		Propeller	
Datapoint	on/off	Speed	Time	CG Location	
1					
2					
3					
4					
5					
6					
7					
8					
9					
10					

A/C		Flight #		Propeller	
Datapoint	on/off	Speed	Time	CG Location	
1					
2					
3					
4					
5					
6					
7					
8					
9					
10					

Appendix C

Complete MATLAB Output Figures

C.1 Low Speed Astraeus

All figures depict the power on neutral point determination unless otherwise noted.

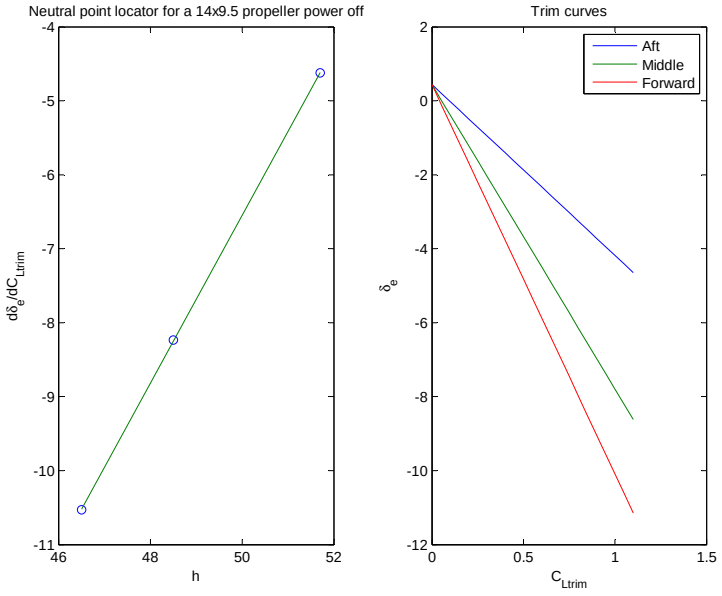

Figure C.1: Design Propeller Power Off Results

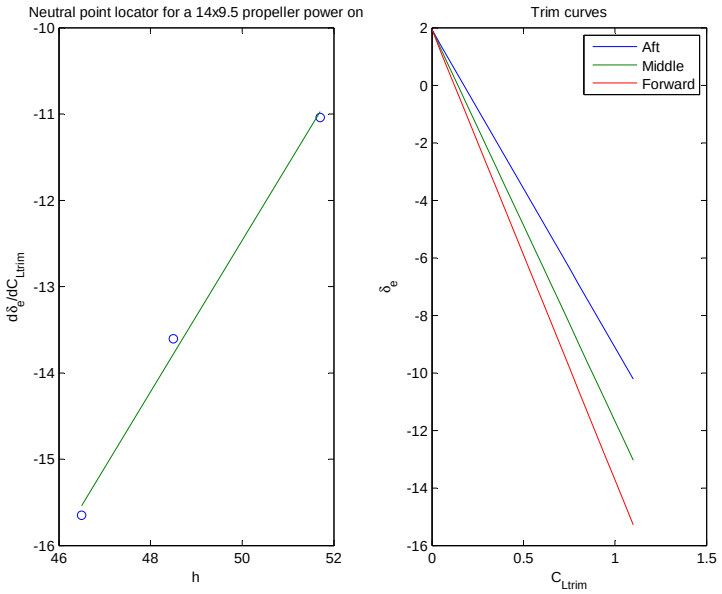

Figure C.2: Design Propeller Power On Results

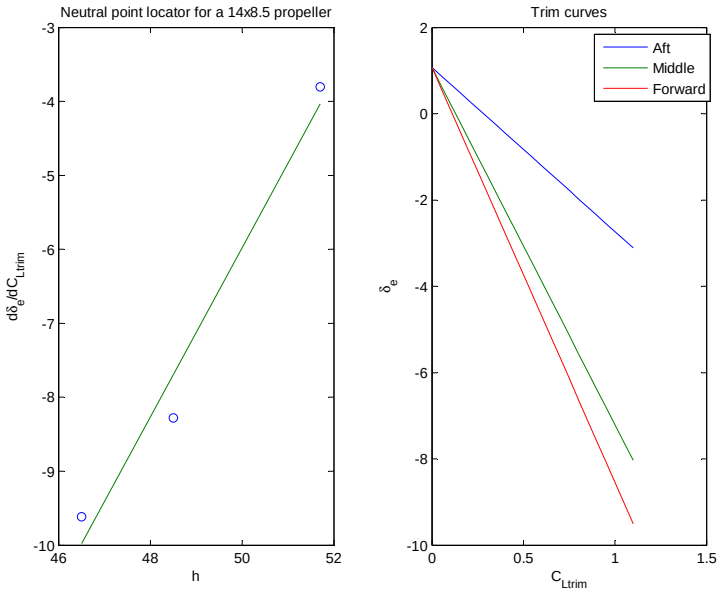

Figure C.3: 14x8.5 Propeller, 3 Point Analysis

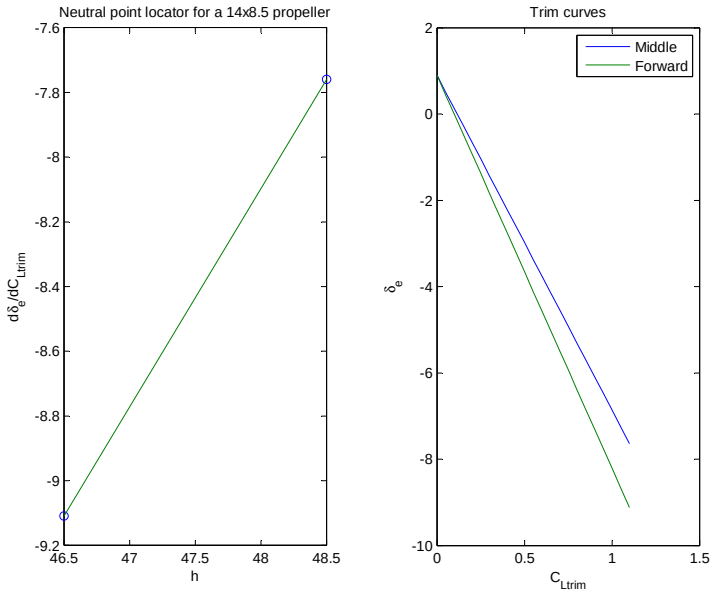

Figure C.4: 14x8.5 Propeller, 2 Point Analysis

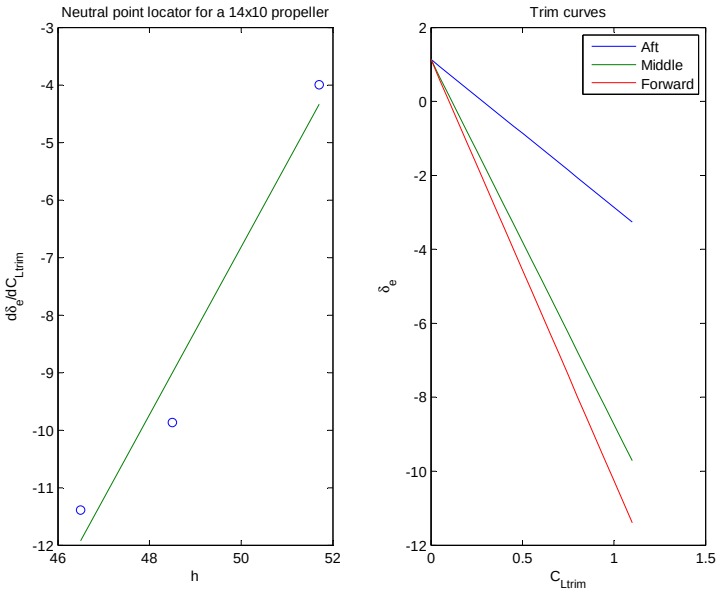

Figure C.5: 14x10 Propeller, 3 Point Analysis

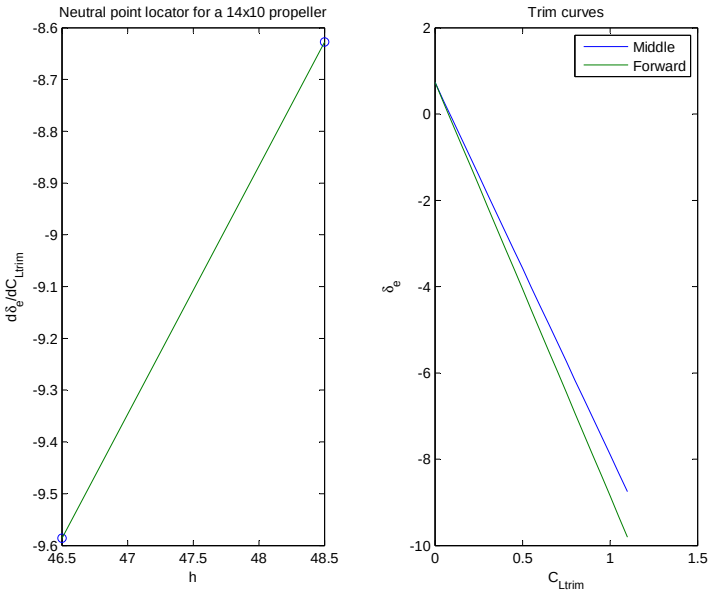

Figure C.6: 14x10 Propeller, 2 Point Analysis

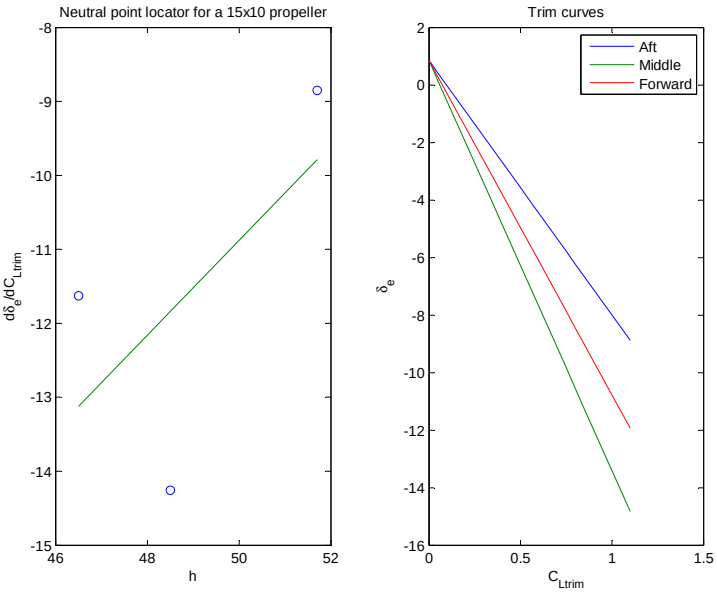

Figure C.7: 15x10 Propeller, 3 Point Analysis

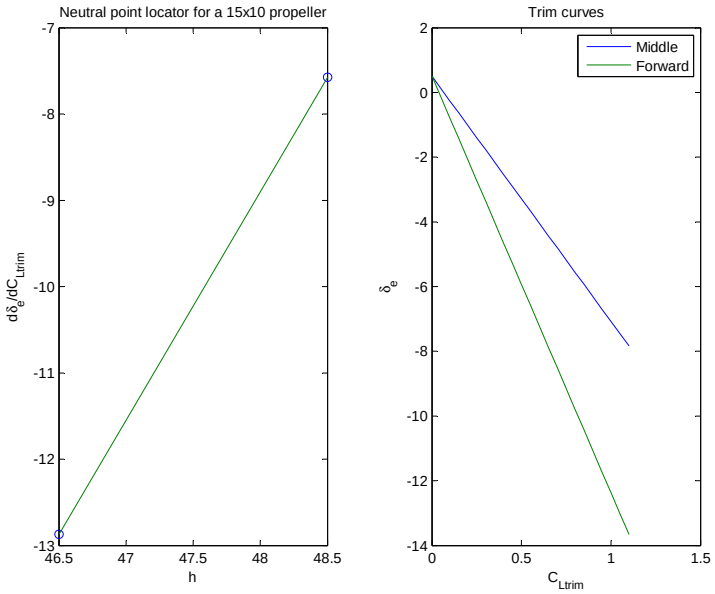

Figure C.8: 15x10 Propeller, 2 Point Analysis

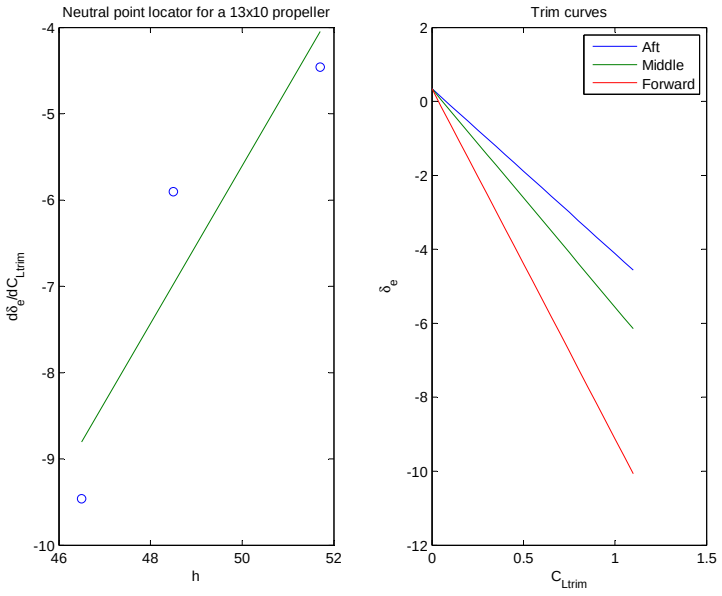

Figure C.9: 13x10 Propeller

C.2 High Speed Astraeus

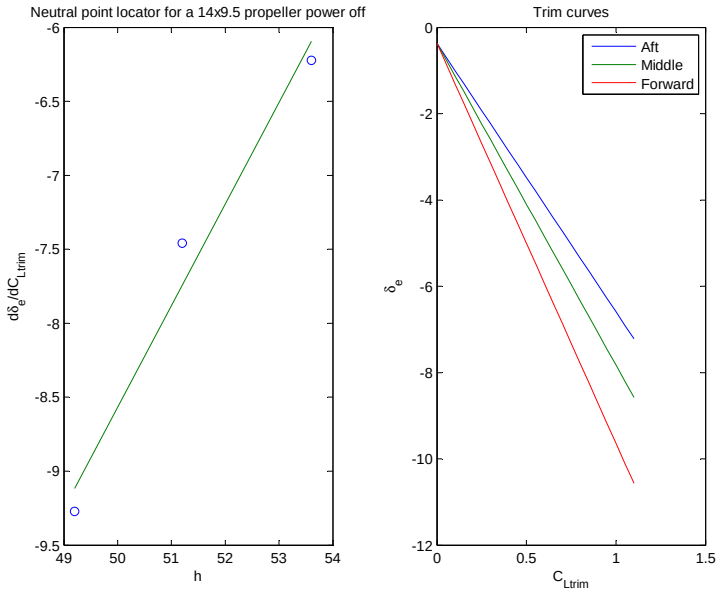

Figure C.10: Design Propeller Power Off Results

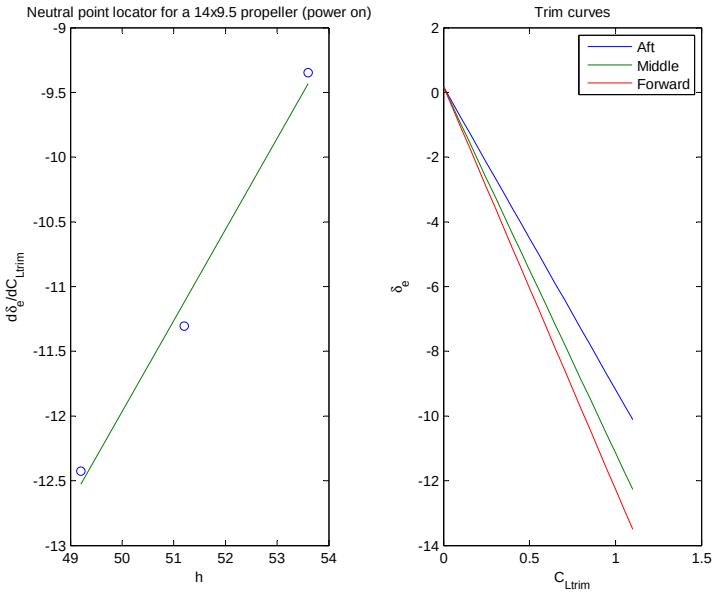

Figure C.11: Design Propeller Power On Results

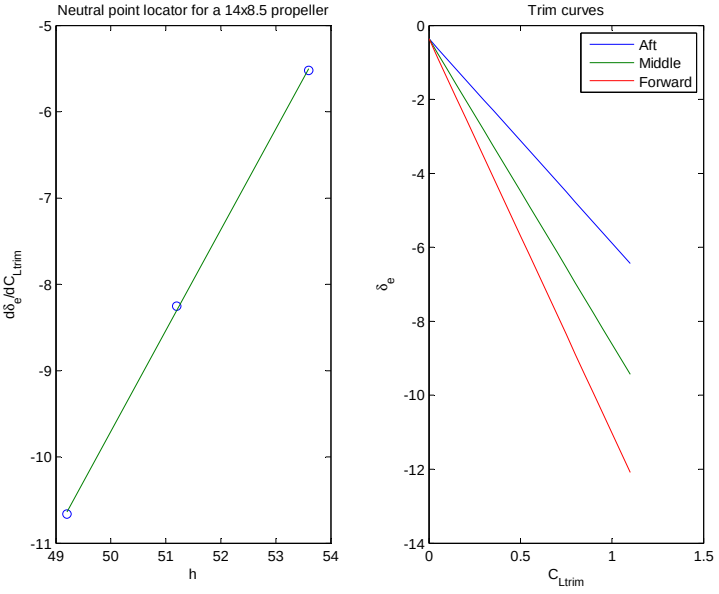

Figure C.12: 14x8.5 Propeller

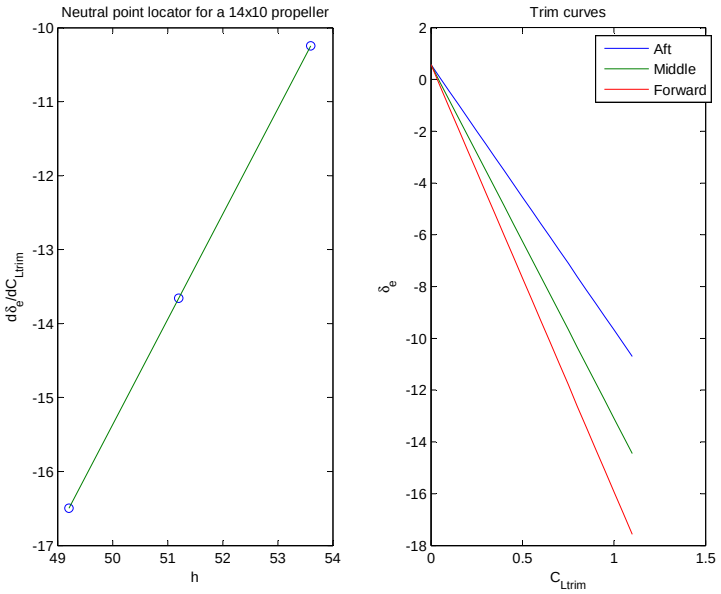

Figure C.13: 14x10 Propeller

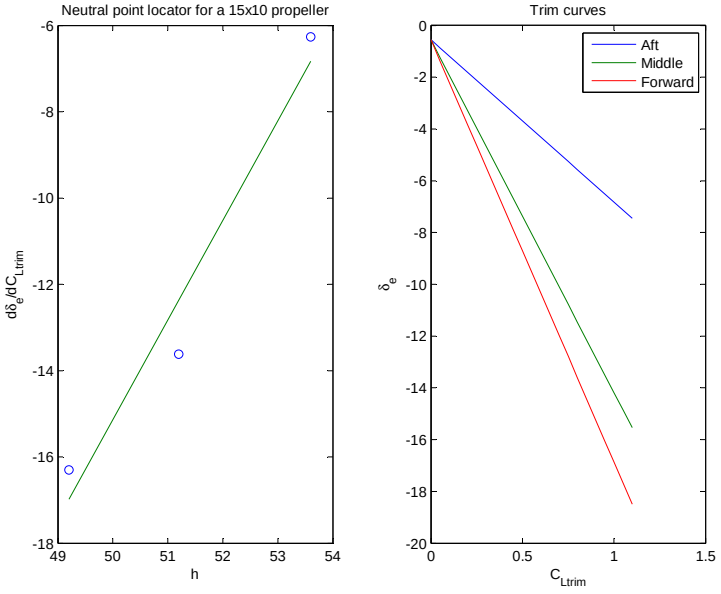

Figure C.14: 15x10 Propeller, 3 Point Analysis

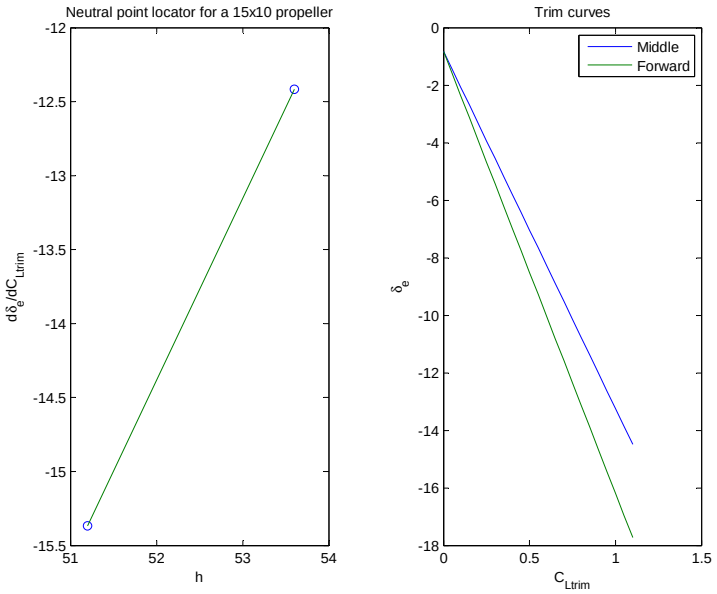

Figure C.15: 15x10 Propeller, 2 Point Analysis

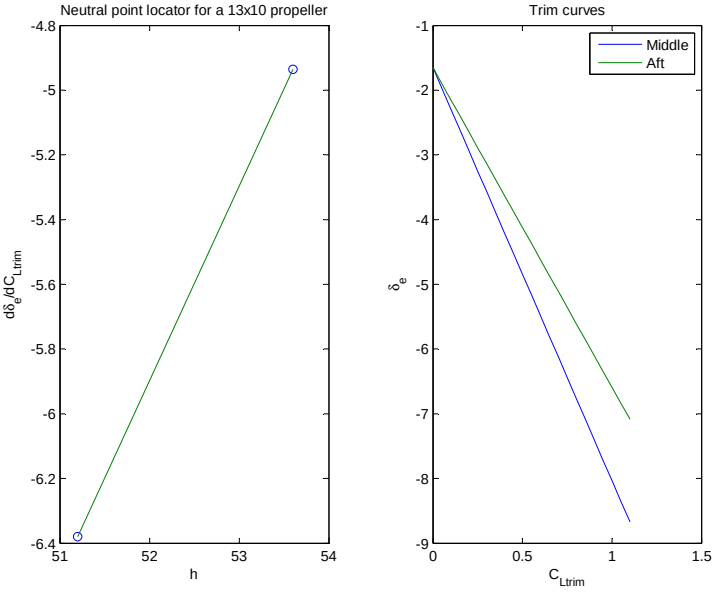

Figure C.16: 13x10 Propeller, 2 Point Analysis

C.3 Optikos

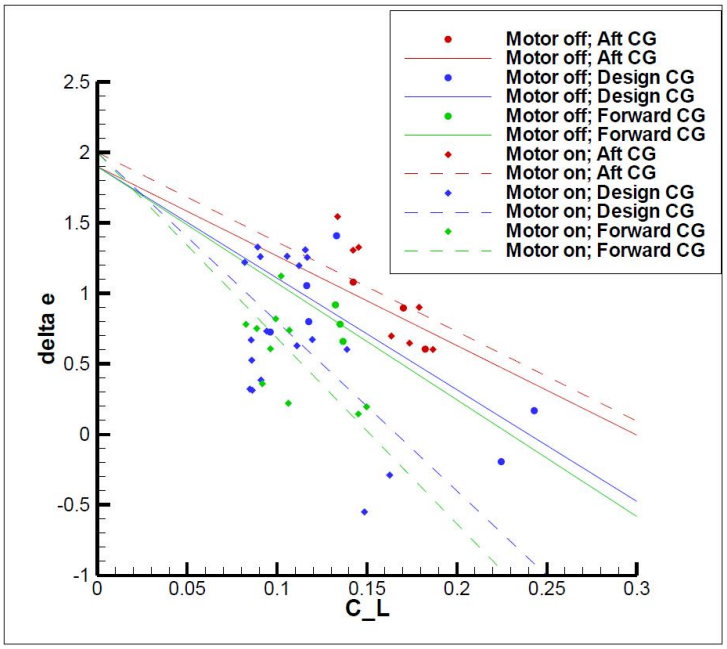

Figure C.17: Optikos Trim Curves

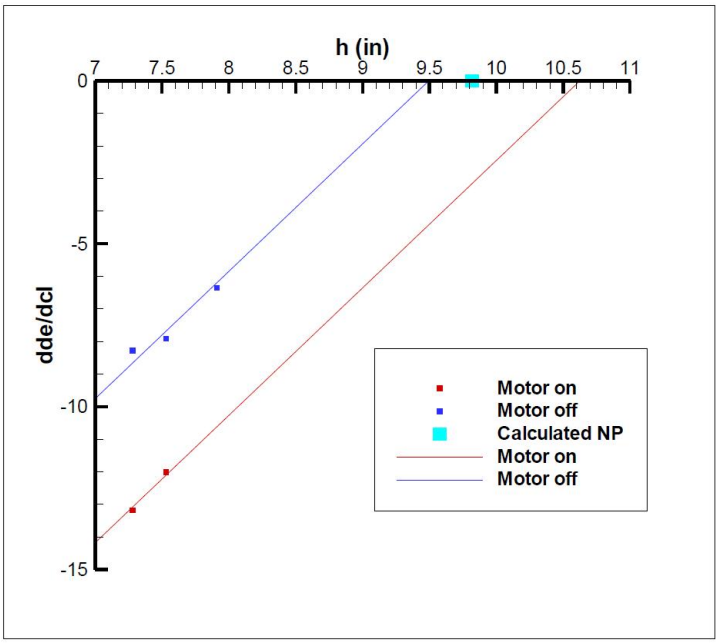

Figure C.18: Optikos h_n Locator

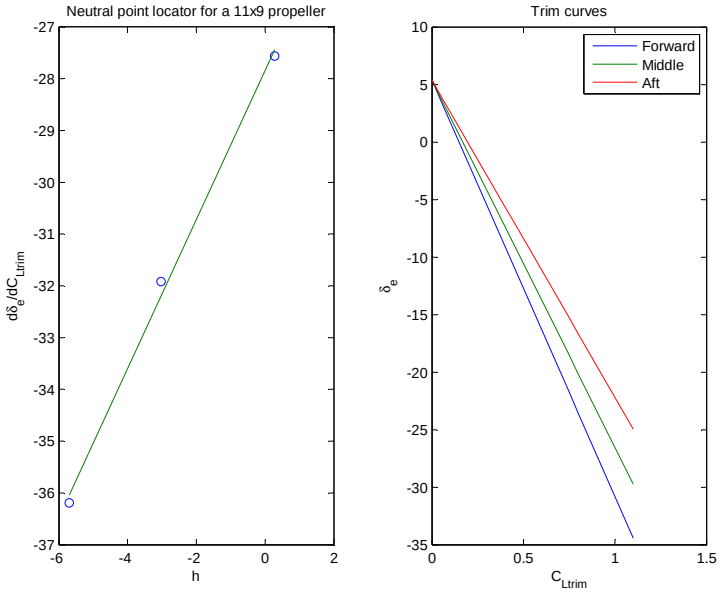

Figure C.19: 11x9 Propeller

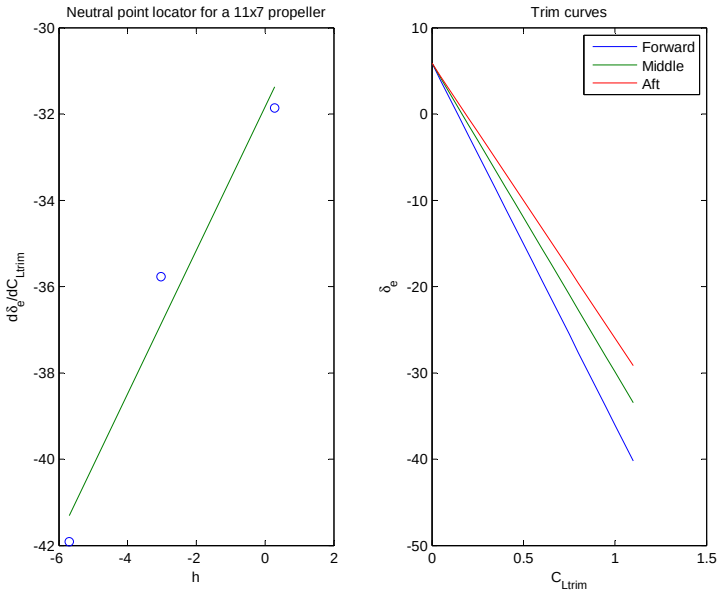

Figure C.20: 11x7 Propeller

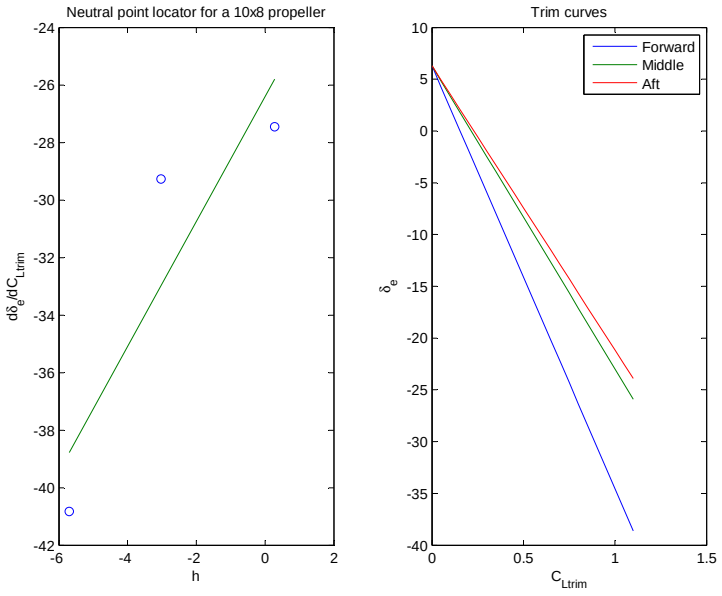

Figure C.21: 10x8 Propeller, 3 Point Analysis

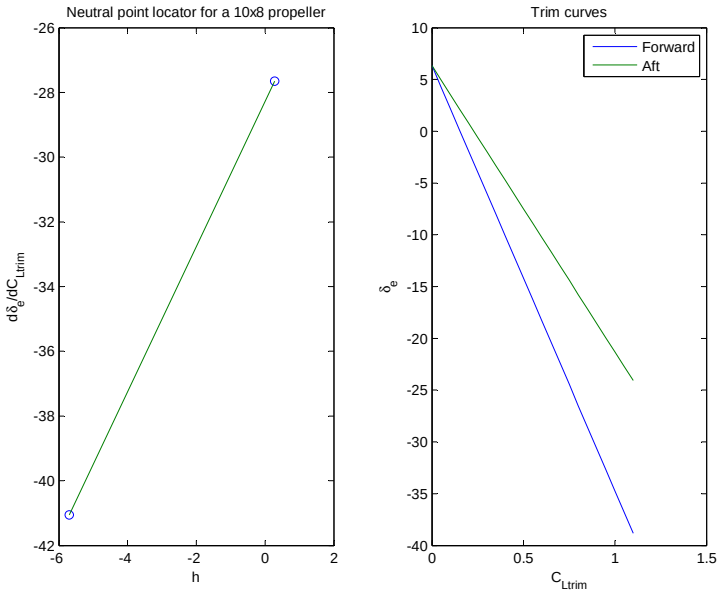

Figure C.22: 10x8 Propeller, 2 Point Analysis

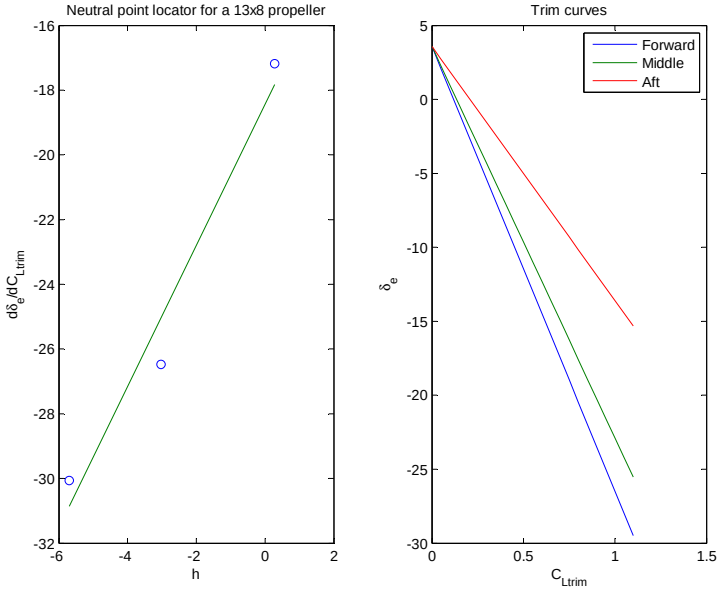

Figure C.23: 13x8 Propeller